symmetry

MDPI

Article

Theoretical Analysis of a COVID-19 CF-Fractional Model to Optimally Control the Spread of Pandemic

Azhar Iqbal Kashif Butt [1,2,†,‡,*], Muhammad Imran [2,‡], Saira Batool [2] and Muneerah AL Nuwairan [1]

[1] Department of Mathematics and Statistics, College of Science, King Faisal University, Al-Ahsa 31982, Saudi Arabia
[2] Department of Mathematics, Government College University, Lahore 54000, Pakistan
* Correspondence: aikhan@kfu.edu.sa
† Current address: Department of Mathematics and Statistics, College of Science, King Faisal University, Al-Ahsa 31982, Saudi Arabia.
‡ These authors contributed equally to this work.

Abstract: In this manuscript, we formulate a mathematical model of the deadly COVID-19 pandemic to understand the dynamic behavior of COVID-19. For the dynamic study, a new SEIAPHR fractional model was purposed in which infectious individuals were divided into three sub-compartments. The purpose is to construct a more reliable and realistic model for a complete mathematical and computational analysis and design of different control strategies for the proposed Caputo–Fabrizio fractional model. We prove the existence and uniqueness of solutions by employing well-known theorems of fractional calculus and functional analyses. The positivity and boundedness of the solutions are proved using the fractional-order properties of the Laplace transformation. The basic reproduction number for the model is computed using a next-generation technique to handle the future dynamics of the pandemic. The local–global stability of the model was also investigated at each equilibrium point. We propose basic fixed controls through manipulation of quarantine rates and formulate an optimal control problem to find the best controls (quarantine rates) employed on infected, asymptomatic, and "superspreader" humans, respectively, to restrict the spread of the disease. For the numerical solution of the fractional model, a computationally efficient Adams–Bashforth method is presented. A fractional-order optimal control problem and the associated optimality conditions of Pontryagin maximum principle are discussed in order to optimally reduce the number of infected, asymptomatic, and superspreader humans. The obtained numerical results are discussed and shown through graphs.

Keywords: COVID-19 epidemic model; CF derivative; existence and uniqueness; Adams–Bashforth computational scheme; optimal control

Citation: Butt, A.I.K.; Imran, M.; Batool, S.; Nuwairan, M.A. Theoretical Analysis of a COVID-19 CF-Fractional Model to Optimally Control the Spread of Pandemic. *Symmetry* **2023**, *15*, 380. https://doi.org/10.3390/sym15020380

Academic Editor: Alexander Zaslavski

Received: 2 January 2023
Revised: 26 January 2023
Accepted: 27 January 2023
Published: 31 January 2023

1. Introduction

COVID-19 is considered a swift-killing infectious disease and has shaken the world to its core. The analysis of global data gathered has proven it to be an acute respiratory syndrome. The first visible appearance was observed in December 2019 in Wuhan, China; afterward, it spread globally, resulting in a pandemic outbreak in 2020 [1]. The COVID-19 pandemic is known as the biggest global pitfall of 2020. It spread fast across different divisions in China. Throughout 2020, the transfer rate of this infection reached its highest point and quickly spread to about 223 nations across the world [2,3]. The deadly virus created a disturbance in the field of medicine and education, ruined people's social lives, and severely damaged economies across the world. Fortunately, Pakistan was affected at a modest rate; it could have been more controlled if more precautionary measures were taken by the country and its people. Different variants of the COVID-19 outbreak were observed in different countries, namely, α, β, γ, and δ. The δ variant is highly contagious, and is 40–60% faster transmissible than the α variant, with a higher risk of health problems [4].

Research has shown that the most common symptoms observed among patients are respiratory problems, breathing issues, coughing, fever, muscular discomfort, fatigue, and severe headaches. Some COVID-19 patients reported experiencing different symptoms, i.e., sore throats, runny noses, sleeping disorders, vomiting, diarrhea, gastroenteritis, and neurological problems of varying severity [5,6]. This disease spreads via contact with infected individuals when they sneeze or cough, or even when via contact with surfaces or objects that already have the virus. The disease's pace of spread accelerated. When we touch our eyes, nose, or mouth with contaminated hands, these delicate parts are contaminated with germs and the germs enter inside the body. Patients with this condition require special care.

Many researchers have formulated different mathematical models to examine the dynamic behaviors of this disease [7–25]. The epidemic compartmental model has symmetry in the sense that the differential equations of the model are developed on the principle that the rate of change of individuals in a particular compartment is equal to the inflow of individuals minus the outflow of individuals. The relevance of the description of epidemic models (to symmetry and asymmetry concepts with interpretations) can be found in [10,26]. Mathematical modeling is a key technique used for studying infectious diseases. Mathematical models and their analyses help in understanding disease transmission mechanisms and in efficiently controlling the spread of diseases. These models assist decision-makers and public health planners in many ways to analyze and control infectious diseases in a population. Recently, many mathematical models have been developed to study the transmission dynamics of COVID-19; see, for example, [27–29]. Initially, these models were based on integer-order derivatives. Experimental and field measurement data cannot be accurately described by integer-order models. Additionally, the integer derivative has a local aspect. As an alternate method, fractional-order models are extensively used. In recent times, researchers have developed an interest in using fractional calculus to analyze real problems in a diverse range of fields, including epidemiological modeling, image processing, chaos theory, and more. Fractional order models (compared to classical order models) integrate memory effects and offer more freedom [30]. Many researchers propose fractional models due to the limitations of ordinary differential equations. A fractional model that involves fractional derivatives makes it simple and accurate to describe physical phenomena that cannot be understood with integer-order derivatives.

Mathematical models with fractional derivatives play an important role in understanding the dynamics of epidemiological diseases. Fractional calculus is considered a generalization of classical order derivatives where the integer-order derivative is replaced by the fractional-order derivative [31]. The study of fractional derivatives revealed that the integer-order model is a special case of the fractional-order model and the solution for a fractional-order differential equation must converge to the solution of an integer-order differential equation as the derivative order approaches one. The fractional-order models, due to their descriptions of memory and hereditary characteristics, are more resourceful than integer-order models and, hence, overcome all restraints on the order of differential equations while finding their solutions. However, the phenomena, which are connected with memory properties and are affected by the hereditary properties, cannot be expressed by the integer-order system. There are many fields where fractional-order systems are more suitable than integer-order systems [32]. The fractional-order COVID-19 infection model has attracted the attention of researchers [33]. Using fractional-order derivatives in the COVID-19 infection model can explain their dynamics more precisely. Thus, researchers noticed the importance of fractional operators with non-singular kernels to better understand the dynamics of physical models. So far, many researchers have explored fractional operators with non-singular kernels, for example, the Caputo–Fabrizio fractional operator and Caputo proportional fractional derivative delay integro-differential equations [34,35]. Keeping the importance of fractional models in mind, we present a CF-fractional COVID-19 model, which is a generalization of the integer-order model given in [36]. The new fractional model will allow us to study the disease dynamics and control more precisely.

There are numerous defined fractional derivatives in the literature; however, this manuscript develops the Caputo–Fabrizio derivative operator with a non-singular exponentially decreasing kernel. In this paper, we present the SEIAPHR fractional model to mathematically examine the coronavirus infection. This research emphasizes the understanding of dynamic behaviors of the disease, preventing its long-term spread. To do this, we demonstrated analytically key characteristics of the suggested fractional model, such as the existence and uniqueness of the solution, the positivity of the solution, invariant region, threshold number, and most significantly, the performed stability analysis. These characteristics provide evidence that we created a feasible model for the COVID-19 epidemic. We will present a modified SEIAPQHR pandemic model in the second half of the paper to examine the effects of quarantine strategies on disease control. The CF-fractional SEIAPQHR model was solved using the Adams–Bashforth technique. An optimal control problem for the suggested fractional model was examined to determine the best quarantine technique. To further illustrate the characteristics of the control problem, various numerical simulations were performed using a projected numerical approach. Based on the numerical results, it can be concluded that the Caputo–Fabrizio operator provides an excellent description and retains system memory effects.

Although people all over the world have been vaccinated, preventative measures are still needed, such as maintaining safe distances from others and wearing face masks, until the proportion of people infected with COVID-19 declines to a safe level. In the wake of the sudden removal of strict pandemic measures, such as travel restrictions and testing of symptomatic and asymptomatic individuals, the virus is again spreading in China at a reasonable speed. Thus, there is a dire need to analyze disease-preventive measures and devise a reasonable control strategy to restrict the spread of the disease. This study also deals with the mathematical and computational analyses of the newly proposed fractional COVID-19 model to study preventive measures in order to suggest an optimal control strategy to minimize the spread of infection.

Our research is divided into seven different sections. In Section 2, preliminaries concerning Caputo–Fabrizio fractional operators and their characteristics are covered in order to develop a nonlinear Caputo–Fabrizio fractional model for the COVID-19 outbreak. Section 3 outlines the theoretical analysis of the proposed fractional model. For instance, by employing the Picard successive iterative approximation method, we demonstrated the existence and uniqueness of a solution. We established two key properties of obtained solutions: boundedness and positivity. The fractional model's equilibrium points are also computed here. The equilibrium points have symmetry, in that the rate of change of the population is zero at these points. Using the next-generation method, we computed the threshold parameter of the model in Section 3. The local and global behaviors of the proposed model at equilibrium points are successfully examined in Section 4. Section 5 presents the modified model. We used the Adams–Bashforth method along with RK-4 to numerically solve the modified system. A comprehensive analysis was done on the effects of the fractional order and quarantine on the model's behavior. Section 6 presents an optimal control analysis. All of the numerical findings are presented with the appropriate explanations and graphic representations. The concluding remarks are given in Section 7.

2. Mathematical Model

In the field of epidemiology, nonlinear models depicting deadly coronavirus transmission patterns are crucial [13–18]. Such models help public health planners and policymakers in a variety of ways. In the existing literature [8–25], there are a variety of mathematical models with varying assumptions based on coronavirus disease transmission. Since integer models are unable to adequately capture the impact of the system's full memory, as well as the scope and spread of the corona infection, we present a novel real-world SEIAPHR fractional pandemic model that takes into account the dynamics of the coronavirus disease transmission.

We identify the total population $N(t)$ into seven compartments: susceptible $S(t)$, exposed $E(t)$, infected $I(t)$, asymptomatic $A(t)$, superspreader $P(t)$, hospitalized $H(t)$, and recovered

$R(t)$. In the susceptible compartment, we consider the individuals who are at risk of being infected. An individual in the susceptible class becomes infected after interacting with an infectious individual and moving to the exposed class $E(t)$. Inhabitants of the exposed class are infected but not infectious yet. Those who become infectious and have symptoms of the disease move to the infected class $I(t)$. The compartment $A(t)$ recruits a group of those infected individuals who are infectious with no disease symptoms. Individuals in the superspreader class are rapid carriers of the disease, e.g., paramedic staff, salespersons, delivery staff, shopkeepers, etc. Infectious people with severe health issues due to the disease move to the hospitalized class $H(t)$. People who recover due to hospital treatment or their robust immune systems are in the recovered class $R(t)$. Thus at any time t,

$$N(t) = S(t) + E(t) + I(t) + A(t) + P(t) + H(t) + R(t). \tag{1}$$

The rate of transmission to the susceptible class is Ψ. Due to interactions between susceptible and infectious individuals, the susceptible are transmitted to the exposed class at the rates γ_1, γ_2, γ_3, and γ_4. The natural mortality rate of all classes is denoted by σ. Exposed individuals transmit at the rates γ_5, γ_6, and γ_7 to the infected $I(t)$, symptomatic $A(t)$, and superspreader $P(t)$ classes, respectively. Infected individuals are hospitalized at the rate of γ_8, recover at the rate of γ_9, and succumb to the disease at a death rate of η_I. Asymptomatic $A(t)$ individuals recover at the rate of τ_1. Superspreaders are hospitalized at the rate of τ_2, recover at the rate of τ_3, and die due to disease at the rate of η_P . The transition rates to the hospitalized class $H(t)$ from the infected $I(t)$ and superspreader $P(t)$ classes are γ_8 and τ_2. The rate of transition from the hospitalized class $H(t)$ to the recovered class $R(t)$ is τ_4. The death rate for the hospitalized class due to the disease is η_H. The transmission rate to the recovered class from the classes $I(t)$, $A(t)$, $P(t)$, and $H(t)$ are γ_9, τ_1, τ_3, and τ_4, respectively. The model variables are assumed to be real-valued functions belonging to $C^1[0, +\infty)$.

We start by going over the basic and auxiliary definitions of the Caputo–Fabrizio fractional operators and their associated characteristics before presenting the fractional model in the sense of the Caputo–Fabrizio derivative.

Definition 1 ([37,38]). *Let $\nu \in H^1(0,T)$, $T > 0$, and $\gamma \in (0,1)$. Then the Caputo–Fabrizio derivative operator of order γ is given by*

$${}_0^{CF}\mathcal{D}_t^{\gamma}\nu(t) = \frac{M(\gamma)}{1-\gamma}\int_0^t \acute{\nu}(s)\ \exp\left[-\frac{\gamma}{1-\gamma}(t-s)\right]ds,\ \ t > 0,$$

where $M(\gamma)$ is the normalization function satisfying the condition $M(0) = M(1) = 1$.

Definition 2 ([37,38]). *Let $\gamma \in (0,1]$, then the associated Caputo–Fabrizio fractional integral operator of order γ is expressed as*

$${}_0^{CF}\mathcal{I}_t^{\gamma}\nu(t) = \frac{2(1-\gamma)}{(2-\gamma)M(\gamma)}\nu(t) + \frac{2(\gamma)}{(2-\gamma)M(\gamma)}\int_0^t \nu(s)ds, \quad t \geq 0. \tag{2}$$

To fully see the internal memory effects of the COVID-19 biological model, we designed a fractional order model that captures the flow pattern described in Figure 1. With the Caputo–Fabrizio derivative operator ${}^{CF}\mathcal{D}_t^{\rho}$ of order $0 < \rho < 1$, the model governing the given flow pattern is presented as:

$$
\begin{aligned}
{}_0^{CF}D_t^{\rho}S(t) &= \Psi - \frac{(\gamma_1 I + \gamma_2 A + \gamma_3 P + \gamma_4 H)S}{N} - \sigma S, && \text{(3a)}\\
{}_0^{CF}D_t^{\rho}E(t) &= \frac{(\gamma_1 I + \gamma_2 A + \gamma_3 P + \gamma_4 H)S}{N} - (\gamma_5 + \gamma_6 + \gamma_7 + \sigma)E, && \text{(3b)}\\
{}_0^{CF}D_t^{\rho}I(t) &= \gamma_5 E - (\gamma_8 + \gamma_9 + \sigma + \eta_I)I, && \text{(3c)}\\
{}_0^{CF}D_t^{\rho}A(t) &= \gamma_6 E - (\tau_1 + \sigma)A, && \text{(3d)}\\
{}_0^{CF}D_t^{\rho}P(t) &= \gamma_7 E - (\tau_2 + \tau_3 + \sigma + \eta_P)P, && \text{(3e)}\\
{}_0^{CF}D_t^{\rho}H(t) &= \gamma_8 I + \tau_2 P - (\tau_4 + \eta_H + \sigma)H, && \text{(3f)}\\
{}_0^{CF}D_t^{\rho}R(t) &= \gamma_9 I + \tau_1 A + \tau_3 P + \tau_4 H - \sigma R, && \text{(3g)}
\end{aligned}
$$

along with the initial conditions

$$S_0 \geq 0,\ E_0 \geq 0,\ I_0 \geq 0,\ A_0 \geq 0,\ P_0 \geq 0,\ H_0 \geq 0,\ R_0 \geq 0, \quad \text{(3h)}$$

where $0 \leq t \leq t_f < \infty$. Suppose that

$$
\begin{aligned}
g_1(y(t)) &= \Psi - \frac{(\gamma_1 I + \gamma_2 A + \gamma_3 P + \gamma_4 H)S}{N} - \sigma S, && \text{(4a)}\\
g_2(y(t)) &= \frac{(\gamma_1 I + \gamma_2 A + \gamma_3 P + \gamma_4 H)S}{N} - (\gamma_5 + \gamma_6 + \gamma_7 + \sigma)E, && \text{(4b)}\\
g_3(y(t)) &= \gamma_5 E - (\gamma_8 + \gamma_9 + \sigma + \eta_I)I, && \text{(4c)}\\
g_4(y(t)) &= \gamma_6 E - (\tau_1 + \sigma)A, && \text{(4d)}\\
g_5(y(t)) &= \gamma_7 E - (\tau_2 + \tau_3 + \sigma + \eta_P)P, && \text{(4e)}\\
g_6(y(t)) &= \gamma_8 I + \tau_2 P - (\tau_4 + \eta_H + \sigma)H, && \text{(4f)}\\
g_7(y(t)) &= \gamma_9 I + \tau_1 A + \tau_3 P + \tau_4 H - \sigma R. && \text{(4g)}
\end{aligned}
$$

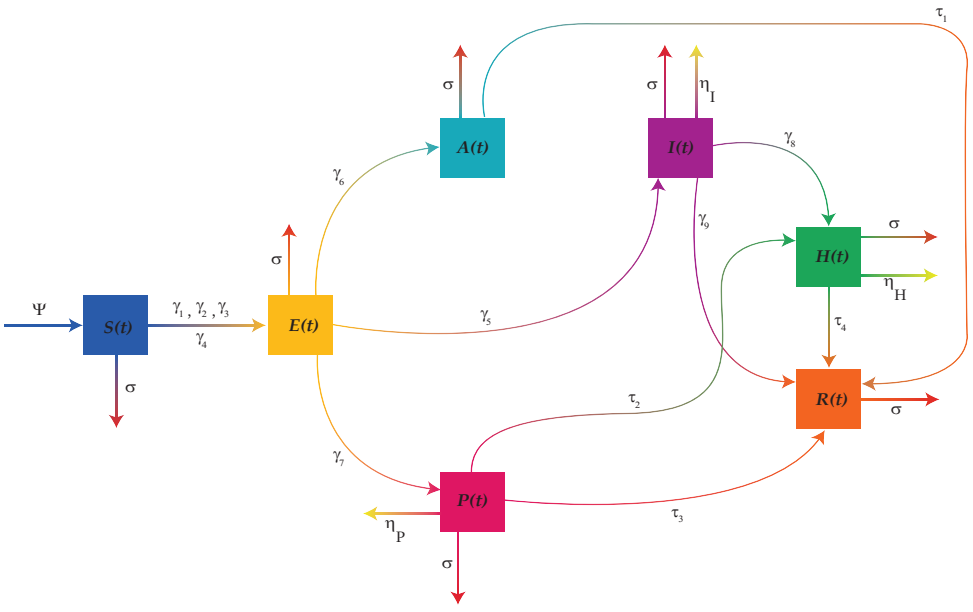

Figure 1. Compartmental view of the disease transmission .

Then, model (3) can be rewritten as

$${}_0^{CF}\mathcal{D}_t^{\rho}y(t) = g(y(t)), \quad y(0) = y_0 \geq 0, \quad \text{(5)}$$

where $g(y(t)) = g_i(y(t))$, $i = 1, \ldots, 7$ is defined in (4), $y(t) = \left(S, E, I, A, P, H, R\right)^T \in \mathbb{R}^7$, $y_0 = \left(S_0, E_0, I_0, A_0, P_0, H_0, R_0\right)^T$ and $g(y(t)) \in C^1[0, t_f]$. The values of the parameters involved in model (3) are shown in Table 1.

Table 1. Parametric values.

Parameter	Description	Values	Reference
γ_1	Transmission rate of S to E after contacting I	0.866	[36]
γ_2	Transmission rate of S to E after contacting A	0.16	[36,39]
γ_3	Transmission rate of S to E after contacting P	0.8	[36]
γ_4	Transmission rate of S to E after contacting H	0.0131	[36,39]
γ_5	Translation of E to I	0.235	[36,39]
γ_6	Translation of E to A	0.26	[36,39]
γ_7	Translation of E to P	0.56	[36]
γ_8	Translation of I to H	0.45	[36,39]
γ_9	Translation of I to R	0.6381	[36,39]
τ_1	Translation of A to R	0.8	[36,39]
τ_2	Translation of P to H	0.1	[36]
τ_3	Translation of P to R	0.3	[36]
τ_4	Translation of H to R	0.54	[36,39]
η_I	Death induced by disease in I	0.08	[36]
η_P	Death induced by disease in P	0.092	[36,39]
η_H	Death induced by disease in H	0.485	[36]
Ψ	Susceptible recruit rate	2.5	[36]
σ	Natural death rate	0.241	[36]

3. Fundamental and Biological Properties

This section deals with the existence and unique results of the Caputo–Fabrizio fractional model (3). The characteristics of the Laplace transformation for the CF-fractional operator are used to prove the boundedness and positivity of the solutions. In this part, the suggested model's reproduction number and two primary equilibrium points are also given.

3.1. Existence and Uniqueness

We employ theorems from functional analyses in this part to demonstrate the existence and uniqueness of the solution.

Theorem 1. *Let $g \in C^1[0, t_f]$, then function $g(y)$ in (5) is Lipschitz continuous.*

Proof. Let V be a convex compact subset of

$$D = \{y(t) | \, 0 \leq t \leq t_f, \, y \in R^7\}.$$

Let $y_1, y_2 \in V$, then by the mean value theorem (MVT) $\exists \, \zeta \in (y_1, y_2)$, such that

$$\frac{g(y_1(t)) - g(y_2(t))}{y_1(t) - y_2(t)} = g^{'}(\zeta(t)),$$

$$g(y_1(t)) - g(y_2(t)) = g^{'}(\zeta(t)).(y_1(t) - y_2(t)),$$

$$\begin{aligned} | \, g(y_1(t)) - g(y_2(t)) \, | &= | \, g^{'}(\zeta(t)).(y_1(t) - y_2(t)) \, |, \\ &\leq \|g^{'}(\zeta)\|_\infty \|y_1 - y_2\|_\infty. \end{aligned}$$

Since $g \in C^1[0, t_f]$, so $\exists$ a constant $\alpha_1 > 0$, such that

$$\|g^{'}(\zeta)\|_\infty \leq \alpha_1.$$

Hence,

$$\begin{aligned} \mid g(y_1(t)) - g(y_2(t)) \mid &\leq \alpha_1 \|y_1 - y_2\|_\infty, \\ \sup_{t\in[0,t_f]} \mid g(y_1) - g(y_2) \mid &\leq \alpha_1 \|y_1 - y_2\|_\infty, \\ \|g(y_1) - g(y_2)\|_\infty &\leq \alpha_1 \|y_1 - y_2\|_\infty. \end{aligned}$$

Thus, $g(y)$ is Lipschitz. □

Theorem 2. *Suppose that the function $g(y)$ satisfies the Lipschitz condition*

$$\|g(y_2) - g(y_1)\|_\infty \leq \alpha_1 \|y_2 - y_1\|_\infty,$$

then the problem (5) has a unique solution for

$$\frac{2\alpha_1}{(2-\rho)M(\rho)}\Big[(1-\rho) + \rho t_f\Big] < 1.$$

Proof. We prove that $y(t)$ is a solution of (5) if and only if it satisfies the equation

$$y(t) = y_0 + \frac{2}{(2-\rho)M(\rho)}\Big[(1-\rho)g(y(t)) + \rho \int_0^t g(y(t))dx\Big]. \tag{6}$$

Let $y(t)$ be the solution of Equation (5). We apply the Caputo–Fabrizio fractional integral (2) to the system (5); that is

$${}^{CF}_{0}I^{\rho}_{t}\Big[{}^{CF}_{0}D^{\rho}_{t}y(t)\Big] = {}^{CF}_{0}I^{\rho}_{t}g(y(t)). \tag{7}$$

We obtain the fractional integral Equation (6).

For converse implication, we let y_n be a sequence of solutions, which converges to solution (6) with the Picard successive iteration, defined as follows:

$$y_n(t) = y_0 + \frac{2}{(2-\rho)M(\rho)}\Big[(1-\rho)g(y_{n-1}(t)) + \rho \int_0^t g(y_{n-1}(x))dx\Big], \quad n = 1, 2, \ldots \tag{8}$$

with $y(t_0) = y_0$.

First, we show that sequence (8) is contractive if

$$k = \frac{2\alpha_1}{(2-\rho)M(\rho)}\Big[(1-\rho) + \rho t_f\Big] < 1.$$

$$\begin{aligned} |y_n(t) - y_{n-1}(t)\ | = | &\frac{2(1-\rho)}{(2-\rho)M(\rho)}[g(y_{n-1}(t)) - g(y_{n-2}(t))] \\ &+ \frac{2\rho}{(2-\rho)M(\rho)}\int_0^t [g(y_{n-1}(x)) - g(y_{n-2}(x))]dx\ |, \\ &\leq \frac{2(1-\rho)}{(2-\rho)M(\rho)}|g(y_{n-1}(t)) - g(y_{n-2}(t))\ | \\ &+ \frac{2\rho}{(2-\rho)M(\rho)}\int_0^t |g(y_{n-1}(x)) - g(y_{n-2})|dx, \end{aligned}$$

using the Lipschitz property of function $g(y)$, we obtain the following expression,

$$\begin{aligned}
|y_n(t) - y_{n-1}(t)\ | &\leq \frac{2(1-\rho)}{(2-\rho)M(\rho)}\alpha_1|y_{n-1}(t) - y_{n-2}(t)\ | \\
&+ \frac{2\rho}{(2-\rho)M(\rho)}\int_0^t \alpha_1|y_{n-1}(t) - y_{n-2}(t)\ |\, dx, \\
&\leq \frac{2(1-\rho)}{(2-\rho)M(\rho)}\alpha_1 \sup_{t\in[0,t_f]}|y_{n-1}(t) - y_{n-2}(t)\ | \\
&+ \frac{2\rho}{(2-\rho)M(\rho)}\int_0^t \alpha_1 \sup_{t\in[0,t_f]}|y_{n-1}(t) - y_{n-2}(t)|dx, \\
|y_n(t) - y_{n-1}(t)\ | &\leq \Big[\frac{2(1-\rho)\alpha_1}{(2-\rho)M(\rho)} + \frac{2\rho\alpha t_f}{(2-\rho)M(\rho)}\Big]\|y_{n-1} - y_{n-2}\|_\infty, \\
\sup_{t\in[0,t_f]}|y_n(t) - y_{n-1}(t)\ | &\leq \Big[\frac{2(1-\rho)\alpha_1}{(2-\rho)M(\rho)} + \frac{2\rho\alpha_1 t_f}{(2-\rho)M(\rho)}\Big]\|y_{n-1} - y_{n-2}\|_\infty, \\
\|y_n - y_{n-1}\|_\infty &\leq k\|y_{n-1} - y_{n-2}\|_\infty.
\end{aligned}$$

This implies

$$d(y_n, y_{n-1}) \leq k\, d(y_{n-1}, y_{n-2}). \tag{9}$$

Thus, from Equation (9), sequence (8) is contractive.
Now for $m, n \in N$ and $m > n$

$$\begin{aligned}
|y_m - y_n\ | &= |y_m - y_{m-1} + y_{m-1} - y_{m-2} + y_{m-2} \ldots - y_{n+1} + y_{n+1} - y_n\ | \\
&\leq |y_m - y_{m-1}\ | + |y_m - 1 - y_{m-2}\ | + \ldots + |y_{n+1} - y_n\ | \\
&\leq k^{m-1}|y_1 - y_0\ | + k^{m-2}|y_1 - y_0\ | + \ldots + k^{m-n}|y_1 - y_0\ | \\
&\leq [k^{m-1} + k^{m-2} + \ldots + k^n]|y_1 - y_0\ |,
\end{aligned}$$

where

$$k = \frac{2\alpha_1}{(2-\rho)M(\rho)}\Big[(1-\rho) + \rho t_f\Big] < 1.$$

Hence, the right-hand side is a geometric series, which is always convergent for $0 < k < 1$.

$$|y_m - y_n\ | \leq k^n \frac{1-k^{m-n}}{1-k}|y_1 - y_0\ | \leq k^n \frac{1}{1-k}|y_1 - y_0\ |\,.$$

Thus, $0 < k < 1$, $lim(k^n) = 0$. Therefore, we infer that sequence (y_n) is Cauchy; hence, it is convergent. Let $lim(y_n) = y$, then Equation (8) gives

$$lim_{n\to\infty} y_n(t) = y(t) = y_0 + \frac{2}{(2-\rho)M(\rho)}\Big[(1-\rho)g(y(t)) + \rho\int_0^t g(y(x))dx\Big]. \tag{10}$$

Equation (10) is the required solution.

Uniqueness: For uniqueness, we suppose that the sequence (y_n) converges to two different limits y_1 and y_2. Then, $n_1, n_2 \in N$, such that,

$$\begin{aligned}
|y_n - y_1\ | &< \epsilon_1\ for\ n_1 \geq n, \\
|y_n - y_2\ | &< \epsilon_2\ for\ n_2 \geq n.
\end{aligned}$$

Let $n = max\{n_1, n_2\}$, then

$$|y_1 - y_2\ | = |y_1 - y_n + y_n - y_2\ | \leq |y_1 - y_n\ | + |y_n - y_2\ | < \epsilon_1 + \epsilon_2 = \epsilon,$$

which implies

$$|y_1 - y_2| = 0 \Rightarrow y_1 = y_2.$$

Hence, the uniqueness of solution (10) of (5) is proved. □

3.2. Boundedness and Positivity of the Solutions

This section is devoted to proving the boundedness and positivity of solutions of the CF-fractional-order model (3) in a feasible region $\Omega = \left\{(S, E, I, A, P, H, R) \in \mathbb{R}_+^7 : 0 < N(t) \leq \frac{\Psi}{\sigma}\right\}$.

Theorem 3. *All solutions of the system (3) are bounded with the given set of non-negative initial conditions* (3h).

Proof. Adding all seven equations of model (3), we have

$$\begin{aligned} {}_0^{CF}\mathcal{D}_t^{\rho} N(t) =& {}_0^{CF}\mathcal{D}_t^{\rho} S(t) + {}_0^{CF}\mathcal{D}_t^{\rho} E(t) + {}_0^{CF}\mathcal{D}_t^{\rho} I(t) \\ &+ {}_0^{CF}\mathcal{D}_t^{\rho} A(t) + {}_0^{CF}\mathcal{D}_t^{\rho} P(t) + {}_0^{CF}\mathcal{D}_t^{\rho} H(t) + {}_0^{CF}\mathcal{D}_t^{\rho} R(t), \\ =& \Psi - (\eta_I I(t) + \eta_P P(t) + \eta_H H(t)) - \sigma N(t), \end{aligned} \tag{11}$$

where $N(t) = S(t) + E(t) + I(t) + A(t) + P(t) + H(t) + R(t)$ is the total population. Clearly,

$$\Psi - (\eta_I I(t) + \eta_P P(t) + \eta_H H(t)) - \sigma N(t) \leq \Psi - \sigma N(t).$$

Therefore, from Equation (11), it follows that

$${}_0^{CF}\mathcal{D}_t^{\rho} N(t) \leq \Psi - \sigma N(t).$$

We apply the Laplace transform on both sides to obtain

$$\mathscr{L}\left[{}_0^{CF}\mathcal{D}_t^{\rho} N(t)\right](s) \leq \frac{\Psi}{s} - \sigma \mathscr{L}[N(t)](s),$$

and further simplification yields us

$$\frac{sN(s)}{s + \rho(1-s)} + \sigma N(s) \leq \Psi s^{-1} + \frac{N(0)}{s + \rho(1-s)},$$

where $N(s) = \mathscr{L}[N(t)](s)$, and $N(0)$ is the total population at $t = 0$.

$$\begin{aligned} N(s) &\leq \frac{\Psi s^{-1}[s + \rho(1-s)] + N(0)}{(1 + \sigma - \sigma\rho)s + \sigma\rho}, \\ N(s) &\leq \frac{\Psi(1-\rho)}{(1 + \sigma - \sigma\rho)s + \sigma\rho} + \frac{\Psi\rho s^{-1}}{(1 + \sigma - \sigma\rho)s + \sigma\rho} + \frac{N(0)}{(1 + \sigma - \sigma\rho)s + \sigma\rho}, \\ N(s) &\leq \frac{\Psi(1-\rho)s^0}{(1 + \sigma - \sigma\rho)\left[s^1 + \frac{\sigma\rho}{(1+\sigma-\sigma\rho)}\right]} + \frac{\Psi\rho s^{1-2}}{(1 + \sigma - \sigma\rho)\left[s^1 + \frac{\sigma\rho}{(1+\sigma-\sigma\rho)}\right]} \\ &\quad + \frac{N(0)}{(1 + \sigma - \sigma\rho)\left[s^1 + \frac{\sigma\rho}{(1+\sigma-\sigma\rho)}\right]}. \end{aligned}$$

Applying the inverse Laplace transformation, we have

$$N(t) \leq \frac{\Psi(1-\rho)}{(1 + \sigma - \sigma\rho)}\mathbb{E}_{1,1}(-\Upsilon t) + \frac{\Psi\rho}{(1 + \sigma - \sigma\rho)} t\mathbb{E}_{1,2}(-\Upsilon t) + \frac{N(0)}{(1 + \sigma - \sigma\rho)}\mathbb{E}_{1,1}(-\Upsilon t), \tag{12}$$

where $\Upsilon = \dfrac{-\sigma\rho}{1+\sigma-\sigma\rho}$, and $\mathbb{E}_{\rho_1,\varrho_1}$ is the Mittag-Leffler function with two parameters $\rho_1 > 0$ and $\varrho_1 > 0$, defined as

$$\mathbb{E}_{\rho_1,\varrho_1}(z) = \sum_{n=0}^{\infty} \frac{z^n}{\Gamma(\rho_1 n + \varrho_1)},$$

whose Laplace transform is given by

$$\mathscr{L}\left[t^{\varrho_1-1}\mathbb{E}_{\rho_1,\varrho_1}(\pm\Lambda t^{\rho_1})\right] = \frac{s^{\rho_1-\varrho_1}}{s^{\rho_1} \mp \Lambda}.$$

The Mittag-Leffler function possesses asymptotic behavior, which we use in inequality (12). Since $N(t) \leq \dfrac{\Psi}{\sigma}$ as $t \to \infty$. Hence, all of the state variables of the model (3) are bounded in Ω. □

It makes no sense to have negative solutions as we are working with a biological model. Thus, the next theorem will demonstrate that for $t > 0$, all state variables of model (3) are positive.

Theorem 4. *For the given set of non-negative initial conditions* (3h)*, the solutions of the system of model (3) are positive.*

Proof. Consider the first equation of the model (3) that can be written as

$${}_0^{CF}\mathcal{D}_t^{\rho} S(t) = \Psi - \left(\frac{\gamma_1 I + \gamma_2 A + \gamma_3 P + \gamma_4 H}{N} + \sigma\right) S.$$

Since all solutions are bounded, we let $I(t)$, $A(t)$, $P(t)$, $H(t)$ and $N(t)$ are bounded by δ_1, δ_2, δ_3, δ_4, and δ_5, respectively. Then,

$${}_0^{CF}\mathcal{D}_t^{\rho} S(t) \geq -mS(t), \tag{13}$$

where $m = \sup\left(\dfrac{\gamma_1\delta_1 + \gamma_2\delta_2 + \gamma_3\delta_3 + \gamma_4\delta_4}{\delta_5} + \sigma\right)$ is a non-negative constant. Taking the Laplace transform on both sides of Equation (13), we have

$$\begin{aligned}
\frac{s\mathscr{L}[S(t)] - S(0)}{s + \rho(1-s)} &\geq -m\mathscr{L}[S(t)], \\
\mathscr{L}[S(t)] &\geq \frac{S(0)}{(1+m-mp)[s + \frac{m\rho}{1+m-m\rho}]}, \\
\mathscr{L}[S(t)] &\geq \frac{S(0)}{(1+m-mp)} \mathscr{L}\left[\mathbb{E}_{1,1}\left\{-\frac{m\rho}{1+m-m\rho}t\right\}\right].
\end{aligned}$$

The application of the inverse Laplace transform on both sides yields

$$S(t) \geq \frac{S(0)}{(1+m-mp)} \left[\mathbb{E}_{1,1}\left\{-\frac{m\rho}{1+m-m\rho}t\right\}\right]. \tag{14}$$

Since $S(0) \geq 0$, and $0 \leq \mathbb{E}_{1,1} \leq 1$, from (14) it is concluded that $S(t) \geq 0$ for all $t \geq 0$. In the same way, the positivity of $E(t)$, $I(t)$, $A(t)$, $P(t)$, $H(t)$, $R(t)$ can be proved for $t \geq 0$ with non-negative initial data. Therefore, the solutions in $\mathbb{R}_+^7$ will be positive for all $t \in [0, \infty)$. □

3.3. Equilibrium Points

If we put

$$ {}_0^{CF}\mathcal{D}_t^{\rho} S = {}_0^{CF}\mathcal{D}_t^{\rho} E = {}_0^{CF}\mathcal{D}_t^{\rho} I = {}_0^{CF}\mathcal{D}_t^{\rho} A = {}_0^{CF}\mathcal{D}_t^{\rho} P = {}_0^{CF}\mathcal{D}_t^{\rho} H = {}_0^{CF}\mathcal{D}_t^{\rho} R = 0, $$

model (3) gives two main equilibrium points. The coronavirus-free (or the disease-free equilibrium (DFE)) point is computed as

$$ \mathcal{P}_0 = (S_0, 0, 0, 0, 0, 0, 0), \text{ where } S_0 = \frac{\Psi}{\sigma}, \tag{15} $$

and the endemic equilibrium (EE) point is given as

$$ \mathcal{P}_1 = (S^1, E^1, I^1, A^1, P^1, H^1, R^1), \tag{16} $$

where

$$ S^1 = \Big[\frac{N(\gamma_5+\gamma_6+\gamma_7+\sigma)}{\beta}\Big],\ E^1 = \Big[\frac{\Psi}{\gamma_5+\gamma_6+\gamma_7+\sigma} - \frac{\sigma N}{\beta}\Big], $$
$$ I^1 = \frac{\gamma_5}{k_2}\Big[\frac{\Psi}{\gamma_5+\gamma_6+\gamma_7+\sigma} - \frac{\sigma N}{\beta}\Big],\ A^1 = \frac{\gamma_6}{k_3}\Big[\frac{\Psi}{\gamma_5+\gamma_6+\gamma_7+\sigma} - \frac{\sigma N}{\beta}\Big], $$
$$ P^1 = \frac{\gamma_7}{k_4}\Big[\frac{\Psi}{\gamma_5+\gamma_6+\gamma_7+\sigma} - \frac{\sigma N}{\beta}\Big],\ H^1 = \frac{1}{k_5}\Big[\frac{\gamma_8\gamma_5}{k_2} + \frac{\tau_2\gamma_7}{k_4}\Big][\frac{\Psi}{\gamma_5+\gamma_6+\gamma_7+\sigma} - \frac{\sigma N}{\beta}\Big], $$
$$ R^1 = \frac{1}{\sigma}\Big[\gamma_9 I^1 + \tau_1 A^1 + \tau_3 P^1 + \tau_4 H^1\Big], $$

with

$$ \beta = \frac{\gamma_1\gamma_5}{k_2} + \frac{\gamma_2\gamma_6}{k_3} + \frac{\gamma_3\gamma_7}{k_4} + \frac{\gamma_4}{k_5}\left(\frac{\gamma_8\gamma_5}{k_2} + \frac{\tau_3\gamma_7}{k_4}\right),\ k_1 = \gamma_5+\gamma_6+\gamma_7+\sigma, $$
$$ k_2 = \gamma_8+\gamma_9+\sigma+\eta_I,\ k_3 = \tau_1+\sigma,\ k_4 = \tau_2+\tau_3+\sigma+\eta_P,\ k_5 = \tau_4+\sigma+\eta_H. $$

3.4. Basic Reproduction Number

The basic reproduction number, commonly written as $\mathcal{R}_0$, is an epidemiological baseline statistic that reflects the total number of secondary cases created by a single infected individual in a completely susceptible population over an infectious period. The differential equations relating to the classes of exposed (E), symptomatic-infected (I), asymptomatic-infected (A), and hospitalized individuals (H) will be the key focus of this section. We use the next-generation method to compute the value of $\mathcal{R}_0$ as described in [40–43]. The matrix of new infection arrival rates in F and translation rates in V at DFE, are defined as

$$ F = \left(\frac{\partial \mathcal{M}}{\partial x_i}\right)_{\mathcal{P}_0}, \quad i = 1,2,3,4,5, $$
$$ V = \left(\frac{\partial \mathcal{S}}{\partial x_i}\right)_{\mathcal{P}_0}, \quad i = 1,2,3,4,5. $$

where $(x_1, x_2, x_3, x_4, x_5) = (E, I, A, P, H)$ and

$$ \mathcal{M} = \begin{pmatrix} \frac{(\gamma_1 I + \gamma_2 A + \gamma_3 P + \gamma_4 H)S}{N} \\ 0 \\ 0 \\ 0 \\ 0 \end{pmatrix}, \quad \mathcal{S} = \begin{pmatrix} (\gamma_5+\gamma_6+\gamma_7+\sigma)E \\ -\gamma_5 E + (\gamma_8+\gamma_9+\sigma+\eta_I)I \\ -\gamma_6 E + (\tau_1+\sigma)A \\ -\gamma_7 E + (\tau_2+\tau_3+\sigma+\eta_P)P \\ -\gamma_8 I - \tau_2 P + (\tau_4+\eta_H+\sigma)H \end{pmatrix}. $$

We determine the spectral radius of the matrix FV^{-1} to obtain the reproduction number $\mathcal{R}_0$.

$$\mathcal{R}_0 = \frac{\gamma_1\gamma_5k_3k_4k_5 + \gamma_2\gamma_6k_2k_4k_5 + \gamma_3\gamma_7k_2k_3k_5 + \gamma_4\gamma_5\gamma_8k_3k_4 + \gamma_4\gamma_7k_2k_3\tau_2}{k_1k_2k_3k_4k_5}. \tag{17}$$

4. Stability Analysis

In this part, we theoretically use $\mathcal{R}_0$ to examine the local stability and global stability of model (3) at both steady states. To investigate global stability, we use the Lyapunov theory with the LaSalle invariance principle [40–43] and the Castillo-Chavez theory [39,44].

4.1. Local Behavior of the Model

To evaluate the local stability of model (3) at DFE, the Jacobian matrix approach is used. The following theorem gives the local stability of model (3) at $\mathcal{P}_0$.

Theorem 5. *Model (3) is locally asymptotically stable (LAS) at $\mathcal{P}_0$ if $\mathcal{R}_0 < 1$ and unstable for $\mathcal{R}_0 > 1$.*

Proof. We compute Jacobian at $\mathcal{P}_0$ for the system (3) to give:

$$J_{\mathcal{P}_0} = \begin{pmatrix} -\sigma & 0 & -\gamma_1 & -\gamma_2 & -\gamma_3 & -\gamma_4 & 0 \\ 0 & -k_1 & \gamma_1 & \gamma_2 & \gamma_3 & \gamma_4 & 0 \\ 0 & \gamma_5 & -k_2 & 0 & 0 & 0 & 0 \\ 0 & \gamma_6 & 0 & -k_3 & 0 & 0 & 0 \\ 0 & \gamma_7 & 0 & 0 & -k_4 & 0 & 0 \\ 0 & 0 & \gamma_8 & 0 & \tau_2 & -k_5 & 0 \\ 0 & 0 & \gamma_9 & \tau_1 & \tau_3 & \tau_4 & -\sigma \end{pmatrix}. \tag{18}$$

We determine the following eigenvalues of the matrix (18).

$$\lambda_1 = -\sigma, \tag{19a}$$
$$\lambda_2 = -\sigma, \tag{19b}$$
$$\lambda_3 = -k_1, \tag{19c}$$
$$\lambda_4 = -\frac{k_1k_2 - \gamma_1\gamma_5}{k_1}, \tag{19d}$$
$$\lambda_5 = -\frac{(k_1k_2k_3k_4k_5)(1-\mathcal{R}_0) + N_1}{k_4k_5(\lambda_3\lambda_4)}, \tag{19e}$$
$$\lambda_6 = -\frac{(1-\mathcal{R}_0)k_1k_2k_3k_4k_5 + N_2}{k_1k_5(\lambda_3\lambda_4)}, \tag{19f}$$
$$\lambda_7 = -\frac{(1-\mathcal{R}_0)}{\lambda_3\lambda_4\lambda_5\lambda_6}, \tag{19g}$$

where,

$$N_1 = k_2k_3k_5\gamma_3\gamma_7 + k_3k_4\gamma_4\gamma_5\gamma_8 + k_2k_3\gamma_4\gamma_7\tau_2,$$
$$N_2 = k_3k_4\gamma_4\gamma_5\gamma_8 + k_2k_3\gamma_4\gamma_7\tau_2.$$

From (19), we observe negativity of all eigenvalues in the case when $\mathcal{R}_0 < 1$. Thus, model (3) is LAS only when $\mathcal{R}_0 < 1$. □

4.2. Global Behavior of the Model

For global stability at $\mathcal{P}_0$, we employ the approach of Castillo-Chavez [44] and used in [39]. We put model (3) in the form

$$\begin{aligned} {}_0^{CF}\mathcal{D}_t^{\rho}\mathcal{X}(t) &= \mathcal{K}(\mathcal{X},\mathcal{Y}), \\ {}_0^{CF}\mathcal{D}_t^{\rho}\mathcal{Y}(t) &= \mathcal{N}(\mathcal{X},\mathcal{Y}), \quad \mathcal{N}(\mathcal{X},0)=0, \end{aligned} \tag{20}$$

where $\mathcal{X}=(S)$ represents the non-infected individuals and $\mathcal{Y}=(E,I,A,P,H)$ represents the infected individuals, with $\mathcal{X}\in\mathbb{R}_+$ and $\mathcal{Y}\in\mathbb{R}_+^5$. Here, we ignored equation (3g) as the state variable R is not involved in any of the equations (3a)–(3f) of a given model. $\mathcal{P}_0=(\mathcal{X}_0,0)=\left(\frac{\Psi}{\sigma},0,0,0,0,0\right)$ is the DFE point. To show global asymptotic stability (GAS) of the disease-free equilibrium point, the conditions given below must be satisfied.

$$(H1)\quad {}_0^{CF}\mathcal{D}_t^{\rho}\mathcal{X}=\mathcal{K}(\mathcal{X},0)=0,\ \mathcal{X}_0 \text{ is } GAS, \tag{21}$$

$$(H2)\quad {}_0^{CF}\mathcal{D}_t^{\rho}\mathcal{Y}=\mathcal{N}(\mathcal{X},\mathcal{Y})=\mathcal{B}\mathcal{Y}-\bar{\mathcal{N}}(\mathcal{X},\mathcal{Y}) \text{ where } \bar{\mathcal{N}}(\mathcal{X},\mathcal{Y})\geq 0 \text{ for all } (\mathcal{X},\mathcal{Y})\in\Omega. \tag{22}$$

Here, $\mathcal{B}=D_{\mathcal{Y}}\mathcal{N}(\mathcal{X}_0,0)$ is an M-matrix and Ω is defined as the feasible region for the model. Thus, for the global stability at DFE, due to Castillo-Chavez et. al. [44], we prove the following theorem.

Theorem 6. *If $\mathcal{R}_0<1$ and the conditions $(H1)$ and $(H2)$ are satisfied, the disease-free equilibrium (DFE) point $\mathcal{P}_0$ of model (3) is globally asymptotically stable (GAS).*

Proof. Let $\mathcal{X}=(S)$ be the uninfected persons, $\mathcal{Y}=(E,I,A,P,H)$ be individuals with infections, and $\mathcal{P}_0=(\mathcal{X}_0,0)$ be the disease-free equilibrium point. Thus,

$${}_0^{CF}\mathcal{D}_t^{\rho}\mathcal{X}=\mathcal{K}(\mathcal{X},\mathcal{Y})=\Psi-(\gamma_1 I+\gamma_2 A+\gamma_3 P+\gamma_4 H)\frac{S}{N}-\sigma S. \tag{23}$$

If $S=S_0$, then $\mathcal{K}(\mathcal{X},0)=0$, i.e.,

$${}_0^{CF}\mathcal{D}_t^{\rho}\mathcal{X}=\Psi-\sigma S_0=0. \tag{24}$$

From Equation (24) as $t\to\infty$, $\mathcal{X}\to\mathcal{X}_0$. Therefore $\mathcal{X}_0=(S_0,0)$ is GAS. Now,

$$\mathcal{B}\mathcal{Y}-\bar{\mathcal{N}}(\mathcal{X},\mathcal{Y})=\begin{bmatrix} -k_1 & \frac{\gamma_1 S_0}{N} & \frac{\gamma_2 S_0}{N} & \frac{\gamma_3 S_0}{N} & \frac{\gamma_4 S_0}{N} \\ \gamma_5 & -k_2 & 0 & 0 & 0 \\ \gamma_6 & 0 & -k_3 & 0 & 0 \\ \gamma_7 & 0 & 0 & -k_4 & 0 \\ 0 & \gamma_8 & 0 & \tau_2 & -k_5 \end{bmatrix}\begin{bmatrix} E \\ I \\ A \\ P \\ H \end{bmatrix}-\begin{bmatrix} \kappa \\ 0 \\ 0 \\ 0 \\ 0 \end{bmatrix}. \tag{25}$$

where

$$\mathcal{B}=\begin{bmatrix} -k_1 & \frac{\gamma_1 S_0}{N} & \frac{\gamma_2 S_0}{N} & \frac{\gamma_3 S_0}{N} & \frac{\gamma_4 S_0}{N} \\ \gamma_5 & -k_2 & 0 & 0 & 0 \\ \gamma_6 & 0 & -k_3 & 0 & 0 \\ \gamma_7 & 0 & 0 & -k_4 & 0 \\ 0 & \gamma_8 & 0 & \tau_2 & -k_5 \end{bmatrix},\quad \mathcal{Y}=\begin{bmatrix} E \\ I \\ A \\ P \\ H \end{bmatrix},\quad \bar{\mathcal{N}}(\mathcal{X},\mathcal{Y})=\begin{bmatrix} \kappa \\ 0 \\ 0 \\ 0 \\ 0 \end{bmatrix},$$

and $\kappa=\dfrac{(\gamma_1 I+\gamma_2 A+\gamma_3 P+\gamma_4 H)}{N}(S_0-S)$.

Here, $\mathcal{B}$ is an M-matrix. Since at $\mathcal{P}_0$, each $S,E,I,A,P,H,R\leq S_0$; thus, matrix $\bar{\mathcal{N}}(\mathcal{X},\mathcal{Y})$ is non-negative. So, point $\mathcal{P}_0$ is GAS. □

Next, we describe the theorem that gives the global stability of the model (3) at $\mathcal{P}_1$.

Theorem 7 ([36–46]). *The endemic equilibrium (EE) point $\mathcal{P}_1$ of model (3) is globally asymptotically stable (GAS) provided $R_0 > 1$ and unstable when $R_0 < 1$.*

Proof. Let us define a Volterra-type Lyapunov function of the form:

$$\begin{aligned}
Ł(S,E,I,A,P,H,R) = &\left[S - S^1 - S^1 \log \frac{S}{S^1}\right] + \left[E - E^1 - E^1 \log \frac{E}{E^1}\right] \\
&+ \left[I - I^1 - I^1 \log \frac{I}{I^1}\right] + \left[A - A^1 - A^1 \log \frac{A}{A^1}\right] \\
&+ \left[P - P^1 - P^1 \log \frac{P}{P^1}\right] + \left[H - H^1 - H^1 \log \frac{H}{H^1}\right] \\
&+ \left[R - R^1 - R^1 \log \frac{R}{R^1}\right].
\end{aligned}$$

with the application of the CF-derivative, the above expression takes the form:

$$\begin{aligned}
{}_0^{CF}\mathcal{D}_t^{\rho} Ł = &\left[\frac{S - S^1}{S}\right] {}_0^{CF}\mathcal{D}_t^{\rho} S + \left[\frac{E - E^1}{E}\right] {}_0^{CF}\mathcal{D}_t^{\rho} E + \left[\frac{I - I^1}{I}\right] {}_0^{CF}\mathcal{D}_t^{\rho} I \\
&+ \left[\frac{A - A^1}{A}\right] {}_0^{CF}\mathcal{D}_t^{\rho} A + \left[\frac{P - P^1}{P}\right] {}_0^{CF}\mathcal{D}_t^{\rho} P \\
&+ \left[\frac{H - H^1}{H}\right] {}_0^{CF}\mathcal{D}_t^{\rho} H + \left[\frac{R - R^1}{R}\right] {}_0^{CF}\mathcal{D}_t^{\rho} R.
\end{aligned} \tag{26}$$

Replacing the derivatives with the right-hand sides of the equations of model (3), we obtain

$$\begin{aligned}
\frac{dŁ}{dt} = &\left[\frac{S - S^1}{S}\right]\left[\Psi - \frac{(\gamma_1 I + \gamma_2 A + \gamma_3 P + \gamma_4 H)S}{N} - (\sigma)S\right] + \left[\frac{E - E^1}{E}\right] \\
&\left[\frac{\gamma_1 I + \gamma_2 A + \gamma_3 P + \gamma_4 H)S}{N}\right] - [(\gamma_5 + \gamma_6 + \gamma_7 + \sigma)E] + \\
&\left[\frac{I - I^1}{I}\right][\gamma_5 - (\gamma_8 + \gamma_9 + \sigma + \eta_I)]I + \left[\frac{A - A^1}{A}\right][\gamma_6 E - (\tau_1 + \sigma)A] + \\
&\left[\frac{P - P^1}{P}\right][\gamma_7 - (\tau_2 + \tau_3 + \sigma + \eta_P)P] + \left[\frac{H - H^1}{H}\right][\gamma_8 I + \tau_2 P - (\tau_4 + \eta_H + \sigma)H] + \\
&\left[\frac{R - R^1}{R}\right][\gamma_9 I + \tau_1 A + \tau_3 P + \tau_4 H - \sigma R].
\end{aligned}$$

We rearrange the terms on the right-hand side to obtain:

$$\begin{aligned}
\frac{d\text{Ł}}{dt} = &\Bigg[\Psi + \left(\frac{(\gamma_1 I + \gamma_2 A + \gamma_3 P + \gamma_4 H)S}{N} + \sigma\right)\frac{(S^1)^2}{S} + \left(\frac{(\gamma_1 I + \gamma_2 A + \gamma_3 P + \gamma_4 H)S}{N}\right)S \\
&+ (\gamma_5 + \gamma_6 + \gamma_7 + \sigma)\frac{(E^1)^2}{E} + \gamma_5 E + (\gamma_8 + \gamma_9 + \sigma + \eta_I)\frac{(I^1)^2}{I} + \gamma_6 E + \gamma_7 E \\
&+ (\tau_1 + \sigma)\frac{(A^1)^2}{A} + (\tau_4 + \eta_H + \sigma)\frac{(H^1)^2}{H} + (\tau_2 + \tau_3 + \eta_P + \sigma)\frac{(P^1)^2}{P} \\
&+ \gamma_8 I + \gamma_9 I + \tau_1 A + \tau_2 P + \tau_3 P + \tau_4 H + \sigma\frac{(R^1)^2}{R}\Bigg] \\
&- \Bigg[\left(\frac{(\gamma_1 I + \gamma_2 A + \gamma_3 P + \gamma_4 H)S}{N} + \sigma\right)\frac{(S - S^1)^2}{S} + \Psi\frac{S^1}{S} \\
&+ \left(\frac{(\gamma_1 I + \gamma_2 A + \gamma_3 P + \gamma_4 H)S}{N} + \sigma\right)S^1 + \frac{(E - E^1)^2}{E}(\gamma_5 + \gamma_6 + \gamma_7 + \sigma) \\
&+ \frac{E^1}{E}\left(\frac{(\gamma_1 I + \gamma_2 A + \gamma_3 P + \gamma_4 H)S}{N}\right)S + (\gamma_5 + \gamma_6 + \gamma_7 + \sigma)E^1 \\
&+ \frac{(I - I^1)^2}{I}(\gamma_8 + \gamma_9 + \eta_I + \sigma) \\
&+ \frac{I^1}{I}\gamma_5 E + (\gamma_8 + \gamma_9 + \sigma + \eta_I)I^1 + (\tau_1 + \sigma)\frac{(A - A^1)^2}{A} + \frac{A^1}{A}\gamma_6 E \\
&+ (\tau_1 + \sigma)A^1 + (\tau_1 + \sigma)A^1 + \frac{(P - P^1)^2}{P}(\tau_2 + \tau_3 + \eta_P + \sigma) + \frac{P^1}{P}\gamma_7 E \\
&+ (\tau_2 + \tau_3 + \eta_P + \sigma)P^1 + \frac{(H - H^1)^2}{H}(\tau_4 + \eta_H + \sigma) + \frac{H^1}{H}(\gamma_8 I + \tau_2 P) \\
&+ (\tau_4 + \eta_H + \sigma)H^1 + \sigma\frac{(R - R^1)^2}{R} + \sigma R^1 + \frac{R^1}{R}(\gamma_9 I + \tau_1 A + \tau_3 P + \tau_4 H)\Bigg].
\end{aligned}$$

Hence, we can write it as:

$$_0^{CF}\mathcal{D}_t^{\rho}\text{Ł} = \xi_1 - \xi_2,$$

where

$$\begin{aligned}
\xi_1 = &\Big[\Psi + (C_1 + \sigma)\frac{(S^1)^2}{S} + C_1 S + (\gamma_5 + \gamma_6 + \gamma_7 + \sigma)\frac{(E^1)^2}{E} + \gamma_5 E \\
&+ (\gamma_8 + \gamma_9 + \sigma + \eta_I)\frac{(I^1)^2}{I} + \gamma_6 E + (\tau_1 + \sigma)\frac{(A^1)^2}{A} + \gamma_7 E \\
&+ (\tau_4 + \eta_H + \sigma)\frac{(H^1)^2}{H} + (\tau_2 + \tau_3 + \eta_P + \sigma)\frac{(P^1)^2}{P} \\
&+ \gamma_8 I + \gamma_9 I + \tau_1 A + \tau_2 P + \tau_3 P + \tau_4 H + \sigma\frac{(R^1)^2}{R}\Big],
\end{aligned}$$

and

$$\begin{aligned}\xi_2 = \Big[&(C_1+\sigma)\frac{(S-S^1)^2}{S} + \Psi\frac{S^1}{S} + (C_1+\sigma)S^1 + \frac{(E-E^1)^2}{E}(\gamma_5+\gamma_6+\gamma_7+\sigma)\\ &+ \frac{E^1}{E}C_1S + (\gamma_5+\gamma_6+\gamma_7+\sigma)E^1 + \frac{(I-I^1)^2}{I}(\gamma_8+\gamma_9+\eta_I+\sigma)\\ &+ \frac{I^1}{I}\gamma_5 E + (\gamma_8+\gamma_9+\sigma+\eta_I)I^1 + (\tau_1+\sigma)\frac{(A-A^1)^2}{A} + \frac{A^1}{A}\gamma_6 E\\ &+ (\tau_1+\sigma)A^1 + (\tau_1+\sigma)A^1 + \frac{(P-P^1)^2}{P}(\tau_2+\tau_3+\eta_P+\sigma) + \frac{P^1}{P}\gamma_7 E\\ &+ (\tau_2+\tau_3+\eta_P+\sigma)P^1 + \frac{(H-H^1)^2}{H}(\tau_4+\eta_H+\sigma) + \frac{H^1}{H}(\gamma_8 I+\tau_2 P)\\ &+ (\tau_4+\eta_H+\sigma)H^1 + \sigma\frac{(R-R^1)^2}{R} + \sigma R^1 + \frac{R^1}{R}(\gamma_9 I+\tau_1 A+\tau_3 P+\tau_4 H)\Big].\end{aligned}$$

As the parameters of model (3) are non-negative, we conclude that ${}_0^{CF}\mathcal{D}_t^{\rho}Ł < 0$ when $\xi_1 < \xi_2$ and ${}_0^{CF}\mathcal{D}_t^{\rho}L = 0$ when $\xi_1 = \xi_2$. The case $\xi_1 = \xi_2$ gives $S = S^1$, $E = E^1$, $A = A^1$, $P = P^1$, $I = I^1$, $H = H^1$, and $R = R^1$. So, as per LaSalle's invariance principle, the endemic equilibrium point $\mathcal{P}_1$ is GAS. □

5. Updated Model with the Quarantine Compartment

Quarantining infected individuals is one way to control the spread of the coronavirus. To implement this control strategy, the original model was updated, such that infected, asymptomatic, and superspreaders were quarantined at a rate of c_1, c_2, and c_3, respectively. Quarantined individuals can die from the disease at a rate of η_Q and die naturally at a rate of σ. Those suffering from severe disease symptoms are hospitalized at a rate of c_4. Moreover, they may receive complete COVID-19 immunity at the rate of c_5. As a result, the modified coronavirus model is represented both graphically (see Figure 2) and mathematically as follows:

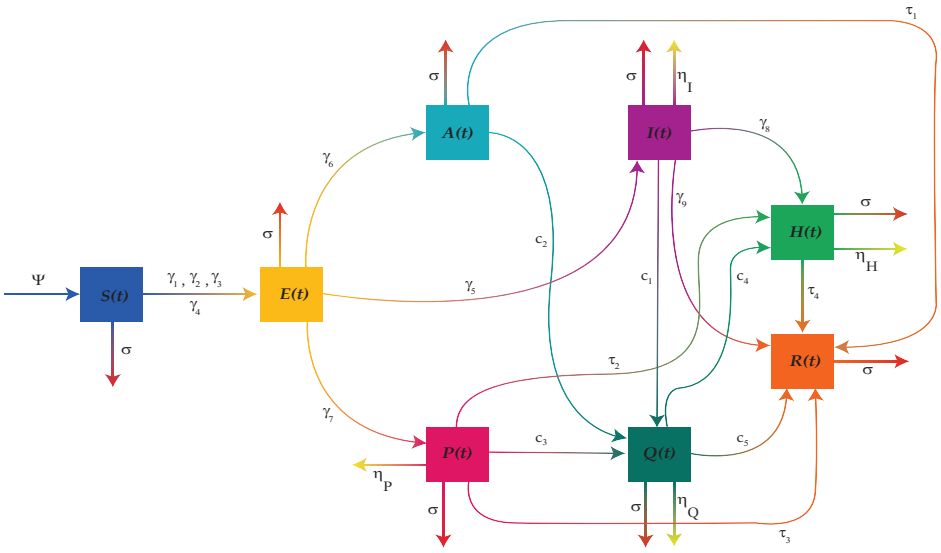

Figure 2. Updated compartmental presentation of disease transmission with the quarantine class.

$$
\begin{aligned}
{}_0^{CF}\mathcal{D}_t^{\rho} S(t) &= \Psi - \frac{(\gamma_1 I(t) + \gamma_2 A + \gamma_3 P + \gamma_4 H)S(t)}{N} - \sigma S(t), && \text{(27a)}\\
{}_0^{CF}\mathcal{D}_t^{\rho} E(t) &= \frac{(\gamma_1 I(t) + \gamma_2 A + \gamma_3 P + \gamma_4 H)S}{N} - (\gamma_5 + \gamma_6 + \gamma_7 + \sigma)E, && \text{(27b)}\\
{}_0^{CF}\mathcal{D}_t^{\rho} I(t) &= \gamma_5 E - (\gamma_8 + \gamma_9 + c_1 + \sigma + \eta_I(t))I(t), && \text{(27c)}\\
{}_0^{CF}\mathcal{D}_t^{\rho} A(t) &= \gamma_6 E - (\tau_1 + c_2 + \sigma)A, && \text{(27d)}\\
{}_0^{CF}\mathcal{D}_t^{\rho} P(t) &= \gamma_7 E - (\tau_2 + \tau_3 + c_3 + \sigma + \eta_P)P, && \text{(27e)}\\
{}_0^{CF}\mathcal{D}_t^{\rho} Q(t) &= c_1 I(t) + c_2 A + c_3 P - (c_4 + c_5 + \eta_Q + \sigma)Q, && \text{(27f)}\\
{}_0^{CF}\mathcal{D}_t^{\rho} H(t) &= \gamma_8 I(t) + \tau_2 P + c_4 Q - (\tau_4 + \eta_H + \sigma)H, && \text{(27g)}\\
{}_0^{CF}\mathcal{D}_t^{\rho} R(t) &= \gamma_9 I(t) + \tau_1 A + \tau_3 P + \tau_4 H + c_5 Q - \sigma R, && \text{(27h)}
\end{aligned}
$$

along with

$$S_0 \geq 0,\ E_0 \geq 0,\ I(t)_0 \geq 0,\ A_0 \geq 0,\ P_0 \geq 0,\ Q_0 \geq 0,\ H_0 \geq 0,\ R_0 \geq 0. \quad \text{(27i)}$$

5.1. Solution Approximating Technique

In this section, we present the numerical technique to solve the model (27). We first discretize the continuous domain $[0, t_f]$ into $\mathcal{N}$ sub-intervals, each of width $\Delta t = \frac{t_f}{\mathcal{N}}$, in order to discretize the state equations of model (27). The discrete points are denoted as $t_i = i\Delta t$, $i = 0, 1, 2, ..., \mathcal{N}$. By using the approximation method described below, we estimate the state equations at these discrete points.

Let us write the Caputo–Fabrizio model (27) in the compact form

$${}_0^{CF}\mathcal{D}_t^{\rho} Z(t) = g(Z),\ \ Z(0) = Z_0,\ \ 0 < \rho \leq 1, \quad \text{(28)}$$

where

$$Z(t) = \big(S(t), E(t), I(t), A(t), P(t), Q(t), H(t), R(t)\big)^T,$$

and

$$g(Z) = \big(g_1(t), g_2(t), g_3(t), g_4(t), g_5(t), g_6(t), g_7(t), g_8(t)\big)^T.$$

We utilized the technique presented in [47] to design an approximation scheme for Equation (28).

Applying the CF-fractional integral operator to both sides of (28), we have

$${}_0^{CF}\mathcal{I}_t^{\rho}\Big({}_0^{CF}\mathcal{D}_t^{\rho} Z(t)\Big) = {}_0^{CF}\ \mathcal{I}_t^{\rho}\Big(g(Z)\Big).$$

This gives

$$Z(t) - Z(0) = \frac{2}{(2-\rho)M(\rho)}\Big[(1-\rho)g(Z) + \rho \int_0^t g(Z(s))ds\Big],$$

and in discrete form

$$Z(t_{i+1}) - Z(0) = \frac{2}{(2-\rho)M(\rho)}\Big[(1-\rho)g(Z(t_i)) + \rho \int_0^{t_{i+1}} g(Z(s))ds\Big]. \quad \text{(29)}$$

Similarly,

$$Z(t_i) - Z(0) = \frac{2}{(2-\rho)M(\rho)}\Big[(1-\rho)g(Z_{i-1}) + \rho\int_0^{t_i} g(Z(s))ds\Big]. \tag{30}$$

From Equations (29) and (30), we obtain

$$Z(t_{i+1}) = Z(t_i) + \frac{2(1-\rho)}{(2-\rho)M(\rho)}\Big[g(Z_i) - g(Z_{i-1})\Big] + \frac{2\rho}{(2-\rho)M(\rho)}\Big[\int_0^{t_{i+1}} g(Z(s))ds - \int_0^{t_i} g(Z(s))ds\Big].$$

This implies that

$$Z_{i+1} = Z_i + \frac{2(1-\rho)}{(2-\rho)M(\rho)}\Big[g(Z_i) - g(Z_{i-1})\Big] + \frac{2\rho}{(2-\rho)M(\rho)}\int_{t_i}^{t_{i+1}} g(Z(s))ds. \tag{31}$$

A Lagrange interpolating polynomial of degree 2 was used to estimate the integral on the right-hand side of (31). That is

$$\begin{aligned}\int_{t_i}^{t_{i+1}} g(Z(s))ds &= \int_{t_i}^{t_{i+1}}\Big[\sum_{m=0}^{2} g(Z(t_{i-m}))L_m(t)ds\Big]dt,\\ &= \Delta t\Big[\frac{23}{12}g(Z(t_i)) - \frac{4}{3}g(Z_{i-1}) + \frac{5}{12}g(Z_{i-2})\Big].\end{aligned} \tag{32}$$

Thus, the iterative scheme (31) in view of (32) takes the form

$$\begin{aligned}Z_{i+1} = Z_i &+ \frac{2}{(2-\rho)M(\rho)}\big(1-\rho+\frac{23}{12}h\rho\big)g(Z_i) - \frac{2}{(2-\rho)M(\rho)}\big(1-\rho+\frac{4}{3}h\rho\big)g(Z_{i-1})\\ &+ \frac{10h\rho}{12(2-\rho)M(\rho)}g(Z_{i-2}), \quad i = 2,3,4,...,\mathcal{N}.\end{aligned} \tag{33}$$

By substituting $\rho = 1$ in Equation (33), the three-step conventional Adam–Bashforth method for an integer-order SEIAPQHR model can be obtained.

5.2. Effect of the Fractional Order on Disease Dynamics

This section explains how the fractional order ρ of model (27) affects COVID-19 transmission dynamics. To study this ρ effect, we implement the finite difference method (33) to obtain graphical results of the proposed fractional model (27) for different fractional orders ρ. Figure 3 illustrates the impact of the arbitrary fractional-order ρ on the number of individuals in one class. For $\rho = 0.7, 0.8, 0.9, 1$, the dynamic behavior of model (27) is simulated. It can be seen that ρ, even at a larger value that is less than 1, has little to no impact on the dynamics of the coronavirus disease. The solution curves appear to function differently in the early stages of the disease for a small duration of time, but beyond some crucial values of time t, they combine to display consistent behavior. The epidemic model's memory effects are unchanged. This implies that changing the value of order ρ as illustrated in Figure 3 will not stop the spread of COVID-19. We can observe that all curves representing susceptibility for different fractional orders stabilize at the same position, i.e., at $S(t) = 8.35$, which is the fraction of the total population in thousands.

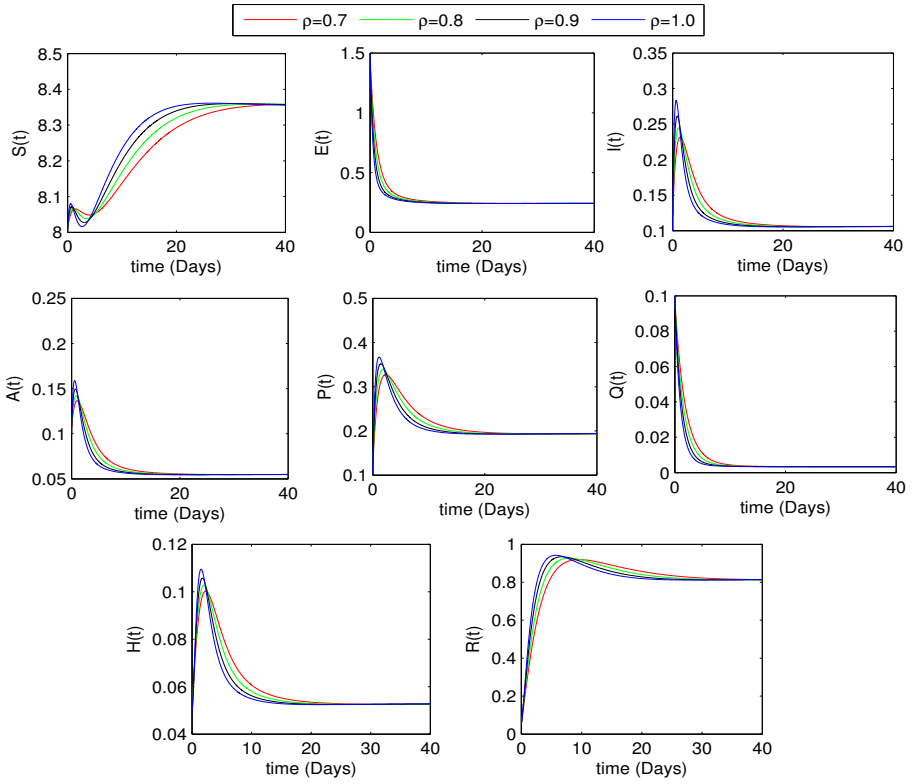

Figure 3. Effects of different fractional orders on the disease dynamics.

5.3. Effect of Quarantine Rates on Disease Dynamics

Using the suggested fractional model (27), we quantitatively investigate the influence of quarantine rates on the dynamics of the coronavirus pandemic in this section. An extended quarantine strategy was intended to control the spread of COVID-19 in the human population. For this, a number of numerical simulations showing the impacts of various quarantine levels are shown, see Figures 4–12. We use the value of the fractional-order ρ as equivalent to 0.7, 0.8, and 0.9 for each considered case. In order to understand the flow pattern and to control the COVID-19 disease, the numerical investigations and observations yielded more conclusive and biologically reasonable results.

It is evident from Figures 4–6 that when the infectious quarantine rate c_1 increases, human populations in all compartments with infections, i.e., in $E,\ I,\ A,\ P,\ H$, except Q decline. Thus, increasing the quarantine rate from compartment $I(t)$ to $Q(t)$, the curve for $I(t)$ will move toward a coronavirus-free state. The quarantine rate c_2 of asymptomatic individuals has relatively less influence on the infected classes $E(t),\ I(t)$, and $P(t)$, compared to classes $A(t)$ and $Q(t)$, where reciprocal behavior is noticed, see Figures 7–9. Almost all other infected compartments remain unchanged with the increase in the quarantine rate c_2. However, we noticed a significant decrease in the solution curves of infected compartments ($E,\ I,\ A,\ P,\ Q,\ and H$) with an increase in the quarantine rate c_3 from the superspreader class $P(t)$. A slightly different behavior of the solution curve of $Q(t)$ can be examined in the beginning. Figures 10–12 show that our developed model moves to DFE in a relatively short period of time when a small number of individuals are isolated from $P(t)$ as opposed to the first two cases. This result is very much valid as the superspreaders are categorized as fast infection-spreading individuals. All scenarios take a 40-day time period into consideration. Since our focus was to study the effects of different quarantine rates on the dynamic behaviors of infections in the population, we omitted the graphs for susceptible $S(t)$ and recovered $R(t)$ individuals under quarantine effects.

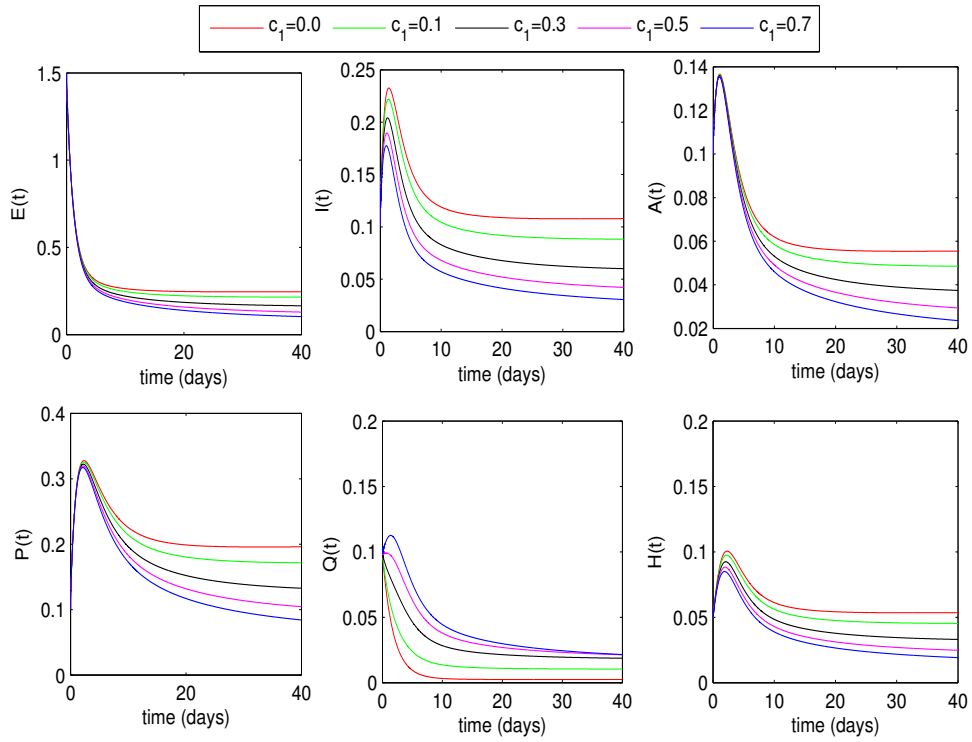

Figure 4. Changing the quarantine rate c_1 from 0% to 70% with $\rho = 0.7$.

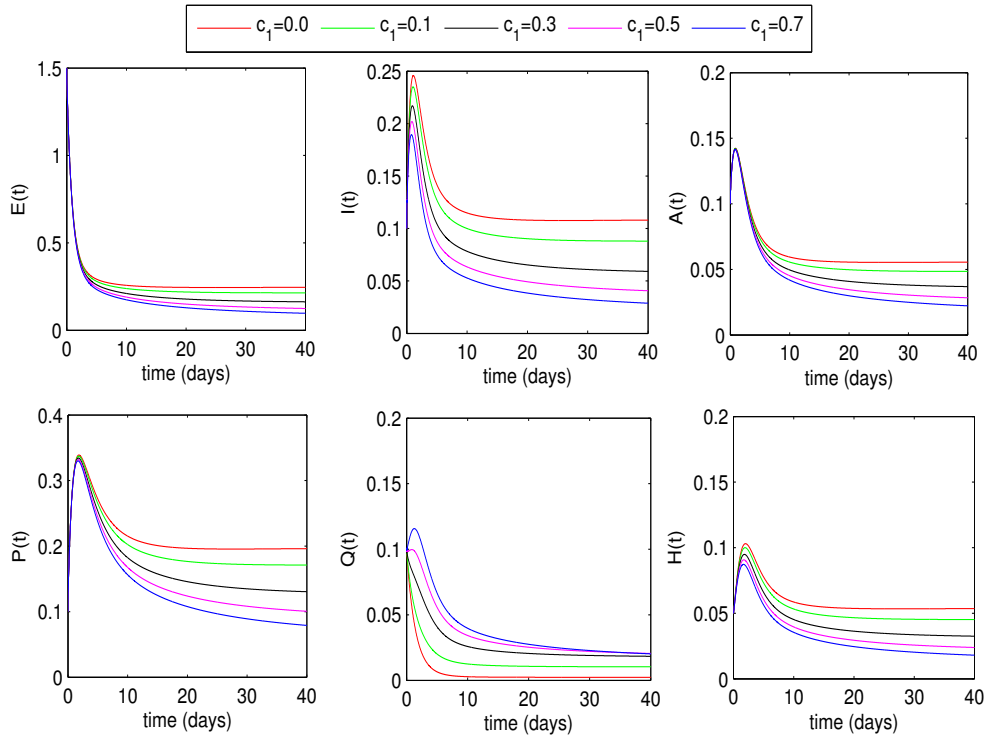

Figure 5. Changing the quarantine rate c_1 from 0% to 70% with $\rho = 0.8$.

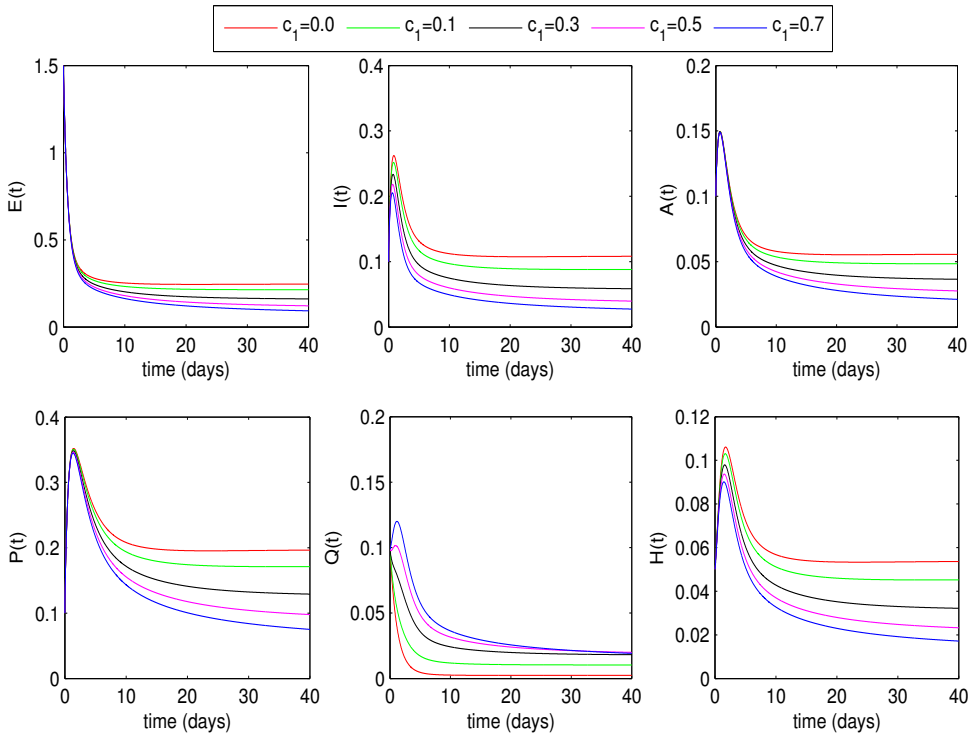

Figure 6. Changing the quarantine rate c_1 from 0% to 70% with $\rho = 0.9$.

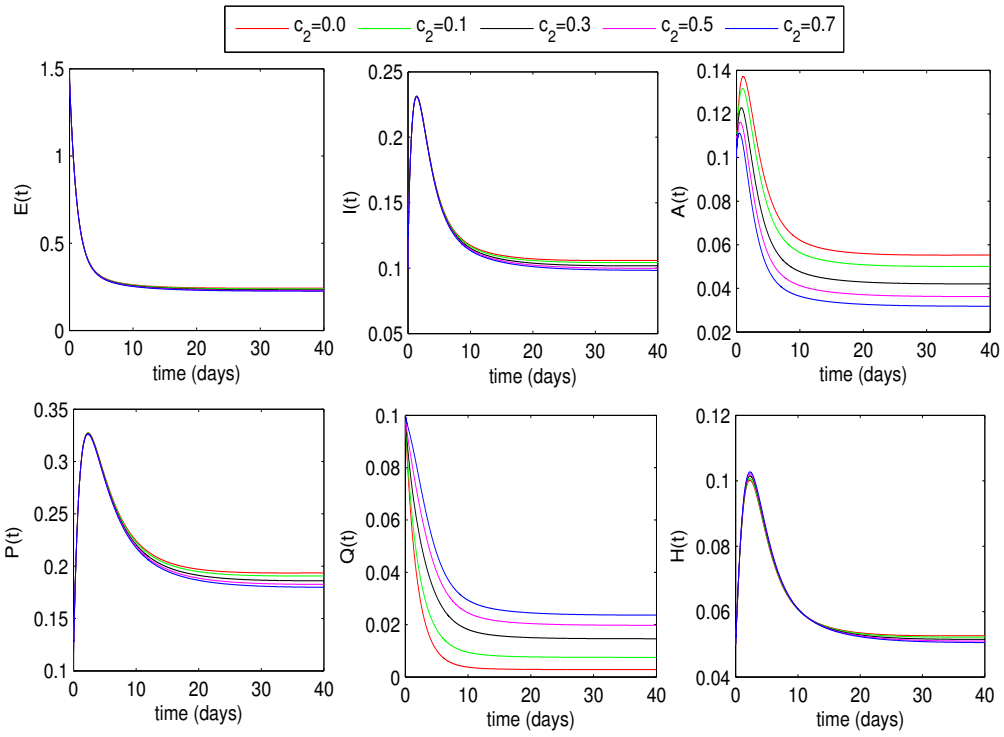

Figure 7. Changing the quarantine rate c_2 from 0% to 70% with $\rho = 0.7$.

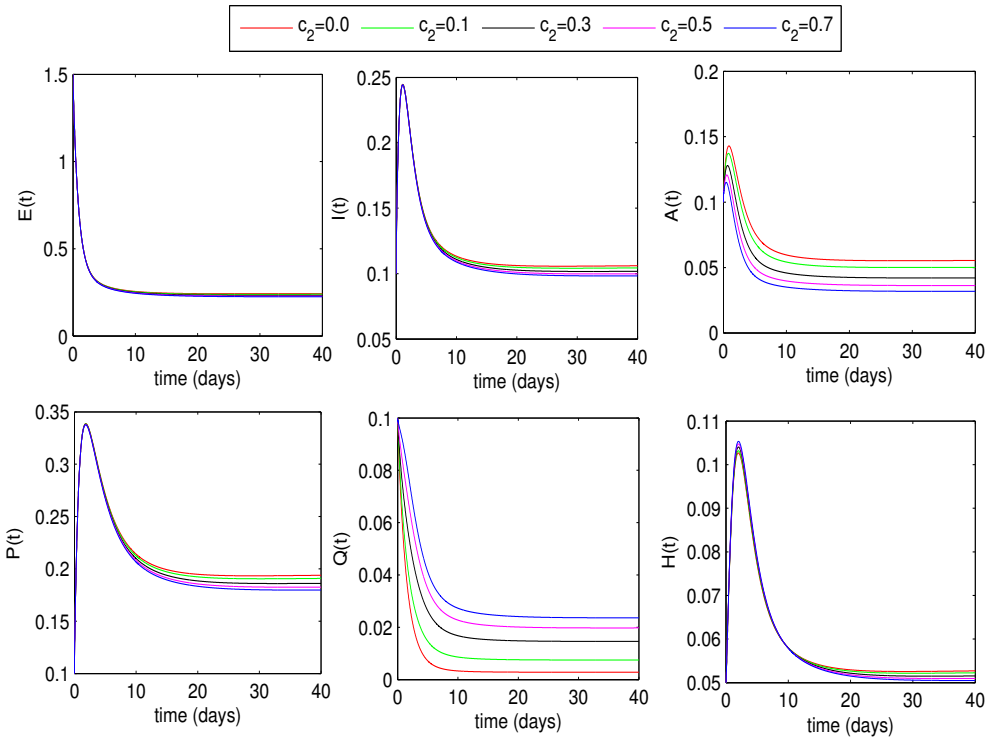

Figure 8. Changing the quarantine rate c_2 from 0% to 70% with $\rho = 0.8$.

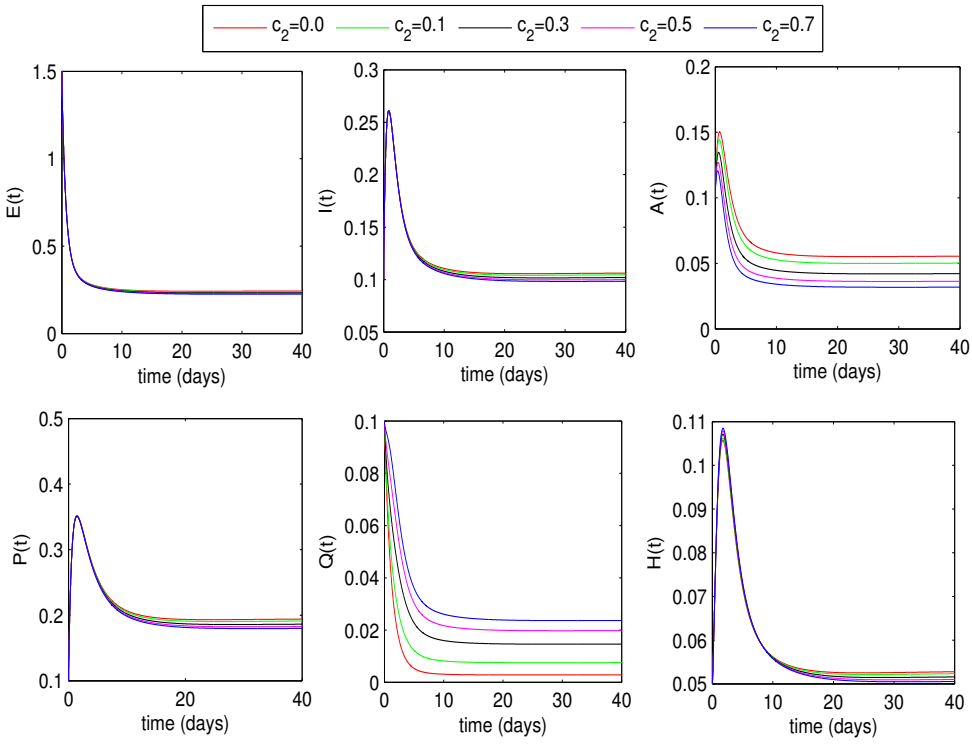

Figure 9. Changing the quarantine rate c_2 from 0% to 70% with $\rho = 0.9$.

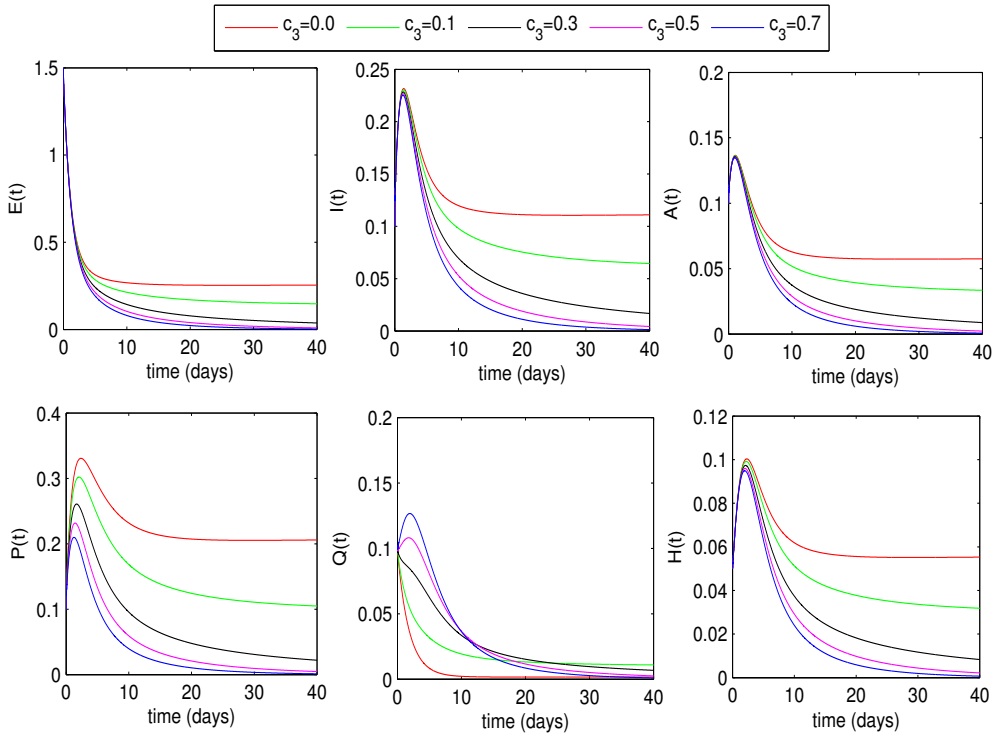

Figure 10. Changing the quarantine rate c_3 from 0% to 70% with $\rho = 0.7$.

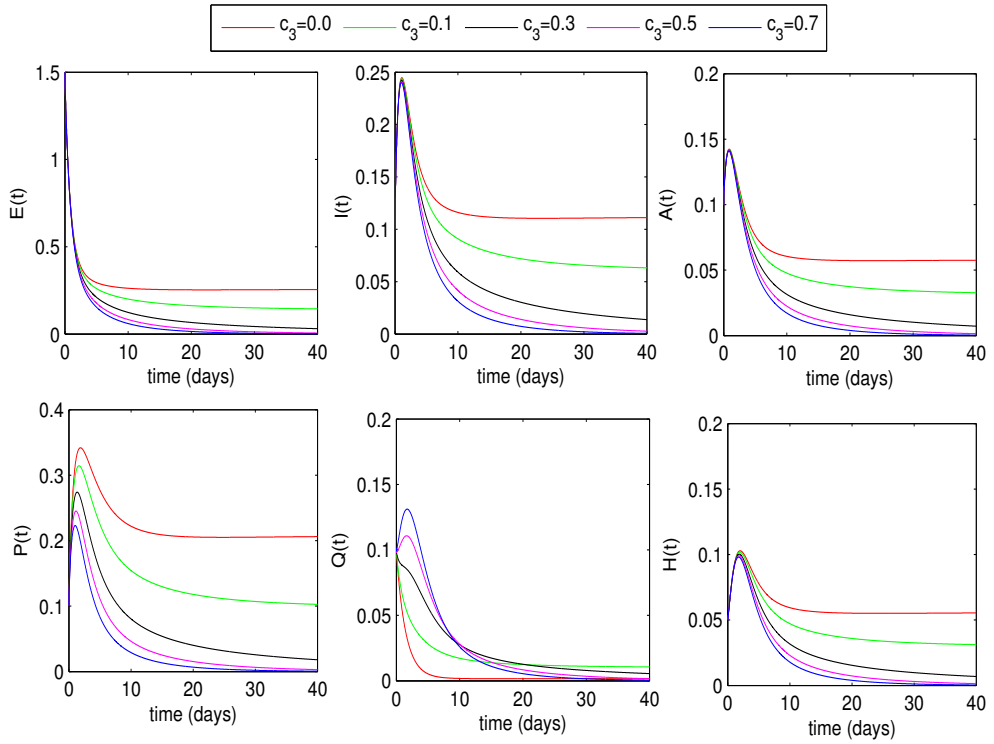

Figure 11. Changing the quarantine rate c_3 from 0% to 70% with $\rho = 0.8$.

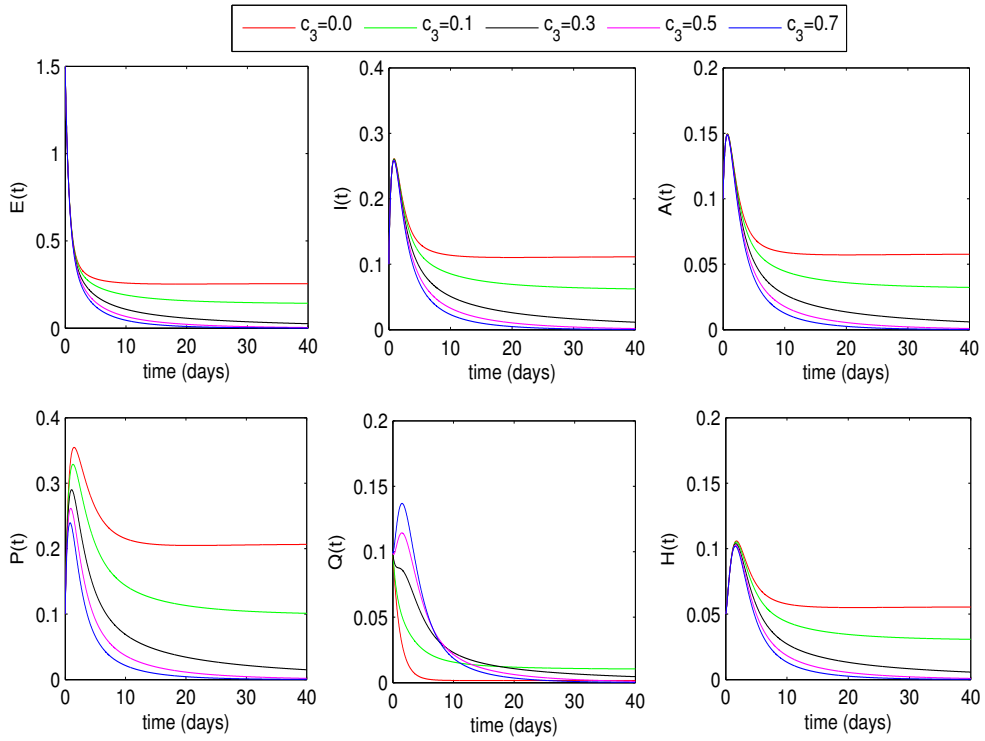

Figure 12. Changing the quarantine rate c_3 from 0% to 70% with $\rho = 0.9$.

6. Formulation of an Optimal Control Problem

Our major purpose was to examine the influences of the quarantine rates of infected, asymptomatic, and superspreader individuals on the spread of the coronavirus disease by applying the best optimal control approach. The goal was to decrease the population of the infected, asymptomatic, and superspreader classes at the lowest possible control costs. In order to identify the potential optimal control in the fractional problem (27), Pontryagin's maximum principle was employed to obtain the necessary conditions. Pontryagin's maximum principle makes it advantageous to adjust the control in the mathematical models in order to attain the required outcomes. In order to control the spread of COVID-19, we applied three control variables described by $u_1(t)$, $u_2(t)$, and $u_3(t)$ to model (27). Quarantine rates $c_1(t)$, $c_2(t)$, and $c_3(t)$ were taken into consideration as the control variables u_1, u_2, and u_3, respectively.

The proposed epidemic model of COVID-19 (with controls) was presented by

$$
\begin{aligned}
{}_0^{CF}\mathcal{D}_t^{\rho} S(t) &= \Psi - \frac{(\gamma_1 I(t) + \gamma_2 A(t) + \gamma_3 P(t) + \gamma_4 H(t))S(t)}{N} - \sigma S(t), && \text{(34a)}\\
{}_0^{CF}\mathcal{D}_t^{\rho} E(t) &= \frac{(\gamma_1 I(t) + \gamma_2 A(t) + \gamma_3 P(t) + \gamma_4 H(t))S(t)}{N} - (\gamma_5 + \gamma_6 + \gamma_7 + \sigma)E, && \text{(34b)}\\
{}_0^{CF}\mathcal{D}_t^{\rho} I(t) &= \gamma_5 E(t) - (\gamma_8 + \gamma_9 + u_1(t) + \sigma + \eta_I)I(t), && \text{(34c)}\\
{}_0^{CF}\mathcal{D}_t^{\rho} A(t) &= \gamma_6 E(t) - (\tau_1 + u_2(t) + \sigma)A(t), && \text{(34d)}\\
{}_0^{CF}\mathcal{D}_t^{\rho} P(t) &= \gamma_7 E(t) - (\tau_2 + \tau_3 + u_3(t) + \sigma + \eta_P)P(t), && \text{(34e)}\\
{}_0^{CF}\mathcal{D}_t^{\rho} Q(t) &= u_1(t)I(t) + u_2(t)A(t) + u_3(t)P(t) - (c_4 + c_5 + \eta_Q + \sigma)Q(t), && \text{(34f)}\\
{}_0^{CF}\mathcal{D}_t^{\rho} H(t) &= \gamma_8 I(t) + \tau_2 P(t) + c_4 Q(t) - (\tau_4 + \eta_H + \sigma)H(t), && \text{(34g)}\\
{}_0^{CF}\mathcal{D}_t^{\rho} R(t) &= \gamma_9 I(t) + \tau_1 A(t) + \tau_3 P(t) + \tau_4 H(t) + c_5 Q(t) - \sigma R(t), && \text{(34h)}
\end{aligned}
$$

along with

$$S(t)_0 \geq 0,\ E(t)_0 \geq 0,\ I(t)_0 \geq 0,\ A(t)_0 \geq 0,\ P(t)_0 \geq 0,\ Q(t)_0 \geq 0,\ H(t)_0 \geq 0,\ R(t)_0 \geq 0. \quad \text{(34i)}$$

To formulate an optimal control problem, the objective cost functional may be defined as

$$J(Z,u) = \int_0^{t_f} \Big[B_1 I(t) + B_2 A(t) + B_3 P(t) + \frac{1}{2}\omega_1 u_1^2(t) + \frac{1}{2}\omega_2 u_2^2(t) + \frac{1}{2}\omega_3 u_3^2(t)\Big] dt, \tag{35}$$

where $I(t)$, $A(t)$, and $P(t)$ are state variables representing the highly infected classes, t_f is the fixed terminal time, and $0 \le u_1(t) \le 1$, $0 \le u_2(t) \le 1$, and $0 \le u_3(t) \le 1$ are the control variables in $[0,1]$. The positive constants B_1, B_2, and B_3 are the associated coefficients for the number of infected, asymptomatic, and superspreader humans, respectively. Moreover, $\frac{1}{2}w_1$, $\frac{1}{2}w_2$, and $\frac{1}{2}w_3$ are the costs of the implemented controls.

To find optimal quarantine strategies to control the coronavirus disease, the assumed control set is given as

$$\mathcal{U} = \Big\{u_1, u_2, u_3 : u_i(t) \text{ is the Lebesgue measurable on [0,1] and } 0 \le u_i(t) \le 1, i = 1,2,3\Big\}.$$

We seek to have admissible optimal controls u_1^*, u_2^*, and u_3^* for the quarantine rates $c_1(t)$, $c_2(t)$, and $c_3(t)$, respectively, in the admissible control function space $\mathcal{U}$, such that the cost function (35) is minimized. That is

$$J^*(I,A,P,u_1^*,u_2^*,u_3^*) = \min_{(u_1,u_2,u_3)\in\mathcal{U}} J(I,A,P,u_1,u_2,u_3) \text{ subject to model (34).} \tag{36}$$

To find the optimal controllers of the fractional optimal control problem (36), we first develop the necessary optimality conditions.

To apply Pontryagin's maximum principle for optimality conditions, we built the Hamiltonian for the control problem (36) as follows:

$$\begin{aligned}
\mathcal{H}(t,Z,\mathcal{U},\zeta) =& B_1 I(t) + B_2 A(t) + B_3 P(t) + \frac{1}{2}\omega_1 u_1^2(t) + \frac{1}{2}\omega_2 u_2^2(t) + \frac{1}{2}\omega_3 u_3^2(t)\\
&+ \zeta_S\left(\Psi - \frac{(\gamma_1 I(t) + \gamma_2 A(t) + \gamma_3 P(t) + \gamma_4 H(t))S(t)}{N(t)} - \sigma S(t)\right)\\
&+ \zeta_E\left(\frac{(\gamma_1 I(t) + \gamma_2 A(t) + \gamma_3 P(t) + \gamma_4 H(t))S(t)}{N(t)} - (\gamma_5 + \gamma_6 + \gamma_7 + \sigma)E(t)\right)\\
&+ \zeta_I(\gamma_5 E(t) - (\gamma_8 + \gamma_9 + u_1(t) + \sigma + \eta_I)I(t))\\
&+ \zeta_A(\gamma_6 E(t) - (\tau_1 + u_2(t) + \sigma)A(t))\\
&+ \zeta_P(\gamma_7 E(t) - (\tau_2 + \tau_3 + u_3(t) + \sigma + \eta_P)P(t))\\
&+ \zeta_Q\big(u_1(t)I(t) + u_2(t)A(t) + u_3(t)P(t) - (c_4 + c_5 + \eta_Q + \sigma)Q(t)\big)\\
&+ \zeta_H(\gamma_8 I(t) + \tau_2 P(t) + c_4 Q(t) - (\tau_4 + \eta_H + \sigma)H(t))\\
&+ \zeta_R(\gamma_9 I(t) + \tau_1 A(t) + \tau_3 P(t) + c_5 Q(t) + \tau_4 H(t) - \sigma R(t)),
\end{aligned} \tag{37}$$

where $Z = (S(t), E(t), I(t), A(t), P(t), Q(t), H(t), R(t))$ symbolize the state variables, ζ_S, ζ_E, ζ_I, ζ_A, ζ_P, ζ_Q, ζ_H, ζ_R, are the associated adjoint variables.

Using the first condition of the Pontryagin principle [48,49], we obtain the equations for controls.

$$\begin{aligned}
\frac{\partial \mathbb{H}}{\partial u_1} = 0 \quad &\Rightarrow \quad u_1(t) = \frac{I(t)(\zeta_I - \zeta_Q)}{\omega_1},\\
\frac{\partial \mathbb{H}}{\partial u_2} = 0 \quad &\Rightarrow \quad u_2(t) = \frac{A(t)(\zeta_A - \zeta_Q)}{\omega_2},\\
\frac{\partial \mathbb{H}}{\partial u_3} = 0 \quad &\Rightarrow \quad u_3(t) = \frac{P(t)(\zeta_P - \zeta_Q)}{\omega_3}.
\end{aligned}$$

Thus, the optimal control characterization for u_1^*, u_2^*, and u_3^* with bounds is given as:

$$u_1^* = min\left\{1, max\left\{0, \frac{I(t)(\zeta_I - \zeta_Q)}{\omega_1}\right\}\right\},$$
$$u_2^* = min\left\{1, max\left\{0, \frac{A(t)(\zeta_A - \zeta_Q)}{\omega_2}\right\}\right\},$$
$$u_3^* = min\left\{1, max\left\{0, \frac{P(t)(\zeta_P - \zeta_Q)}{\omega_3}\right\}\right\}. \tag{38}$$

Using the second optimality condition of PMP, i.e., by differentiating the Hamiltonian (37) with respect to state variables, the adjoint system of the fractional-order differential equation is obtained as:

$$\begin{aligned}
{}_0^{CF}\mathcal{D}^\rho \zeta_S(t) &= -\left(\frac{\gamma_1 I(t) + \gamma_2 A(t) + \gamma_3 P(t) + \gamma_4 H(t)}{N(t)} + \sigma\right)\zeta_S \\
&\quad + \left(\frac{\gamma_1 I(t)\gamma_2 A(t) + \gamma_3 P(t) + \gamma_4 H(t)}{N(t)}\right)\zeta_E, && \text{(39a)}\\
{}_0^{CF}\mathcal{D}^\rho \zeta_E(t) &= -(\gamma_5 + \gamma_6 + \gamma_7 + \sigma)\zeta_E + \gamma_5\zeta_I + \gamma_6\zeta_A + \gamma_7\zeta_P, && \text{(39b)}\\
{}_0^{CF}\mathcal{D}^\rho \zeta_I(t) &= -\left(\frac{\gamma_1 S(t)}{N(t)}\right)\zeta_S + \left(\frac{\gamma_1 S(t)}{N(t)}\right)\zeta_E - (\gamma_8 + \gamma_9 + u_1(t) + \sigma + \eta_I)\zeta_I \\
&\quad + u_1(t)\zeta_Q + \gamma_8\zeta_H + \gamma_9\zeta_R + B_1, && \text{(39c)}
\end{aligned}$$

$$\begin{aligned}
{}_0^{CF}\mathcal{D}^\rho \zeta_A(t) &= -\left(\frac{\gamma_2 S(t)}{N(t)}\right)\zeta_S + \left(\frac{\gamma_2 S(t)}{N(t)}\right)\zeta_E - (\tau_1 + u_2(t) + \sigma)\zeta_A + u_2(t)\zeta_Q + \tau_1\zeta_R + B_2, && \text{(39d)}\\
{}_0^{CF}\mathcal{D}^\rho \zeta_P(t) &= -\left(\frac{\gamma_3 S(t)}{N(t)}\right)\zeta_S + \left(\frac{\gamma_3 S(t)}{N(t)}\right)\zeta_E - (\tau_2 + \tau_3 + u_3(t) + \sigma + \eta_P)\zeta_P \\
&\quad + u_3(t)\zeta_Q + \tau_2\zeta_H + \tau_3\zeta_R + B_3, && \text{(39e)}\\
{}_0^{CF}\mathcal{D}^\rho \zeta_Q(t) &= -(c_4 + c_5 + \eta_Q + \sigma)\zeta_Q + c_4\zeta_H + c_5\zeta_R, && \text{(39f)}\\
{}_0^{CF}\mathcal{D}^\rho \zeta_H(t) &= -\left(\frac{\gamma_4 S(t)}{N(t)}\right)\zeta_S + \left(\frac{\gamma_4 S(t)}{N(t)}\right)\zeta_E - (\tau_4 + \eta_H + \sigma)\zeta_H + \tau_4\zeta_R, && \text{(39g)}\\
{}_0^{CF}\mathcal{D}^\rho \zeta_R(t) &= -\sigma\zeta_R, && \text{(39h)}
\end{aligned}$$

with transversality conditions

$$\zeta_S(t_f) = \zeta_E(t_f) = \zeta_I(t_f) = \zeta_A(t_f) = \zeta_P(t_f) = \zeta_Q(t_f) = \zeta_H(t_f) = \zeta_R(t_f) = 0.$$

6.1. Numerical Study of an Optimal Control Problem

The numerical solutions to an optimal control problem are presented in this subsection. Our goal is to determine the most cost-effective quarantine rates by minimizing the objective functional (35). Consequently, this section explains the optimal control problem's solution together with the associated cost functional. The numerical approaches used to obtain the approximate solutions of Equation (34) and the adjoint Equations (39) are given below.

The iterative scheme (33) used to solve the system of state Equation (34) takes the form

$$\begin{aligned}
Z_{i+1} &= Z_i + \frac{2}{(2-\rho)M(\rho)}(1 - \rho + \frac{23}{12}h\rho)g(Z_i, u_i) - \frac{2}{(2-\rho)M(\rho)}(1 - \rho + \frac{4}{3}h\rho)g(Z_{i-1}, u_{i-1}) \\
&\quad + \frac{10h\rho}{12M(\rho)}g(Z_{i-2}, u_{i-2}), \quad i = 2, 3, 4, ..., \mathcal{N}, && \text{(40)}
\end{aligned}$$

The system of adjoint Equation (39) in compact form can be written as

$$ {}_{0}^{CF}\mathcal{D}_{t}^{\rho}\hat{\zeta}(t_f - t) = F(Z(t_f - t), \hat{\zeta}(t_f - t), u(t_f - t)), $$

where

$$ F(Z,u) = \begin{pmatrix} F_1(Z,u) \\ F_2(Z,u) \\ F_3(Z,u) \\ F_4(Z,u) \\ F_5(Z,u) \\ F_6(Z,u) \\ F_7(Z,u) \\ F_8(Z,u) \end{pmatrix}. $$

Similar to the state equations, the adjoint Equations (39) are discretized as follows:

$$ \begin{aligned} \hat{\zeta}(t_f - t_{i+1}) = \hat{\zeta}(t_f - t_i) &+ \frac{2}{(2-\rho)M(\rho)}\left[1 - \rho + \frac{23}{12}h\rho\right]F(\phi(t_f - t_i), \hat{\zeta}(t_f - t_i), u(t_f - t_i)) \\ &- \frac{2}{(2-\rho)M(\rho)}\left[1 - \rho + \frac{4}{3}h\rho\right]F(\phi(t_f - t_{i-1}), \hat{\zeta}(t_f - t_{i-1}), u(t_f - t_{i-1})) \\ &+ \frac{10h\rho}{12M(\rho)}F(\phi(t_f - t_{i-2}), \hat{\zeta}(t_f - t_{i-2}), u(t_f - t_{i-2})), \end{aligned} \tag{41} $$

with $\hat{\zeta}(t_f) = 0$ where $i = 0, 1, ...\mathcal{N}$. Discrete state and adjoint variables, respectively, given in (40) and (41) are solved first to update the control $u(t)$, at the discrete points $t_i = i\Delta t$.

6.1.1. Solution Algorithm

For the numerical solution of the discrete necessary conditions, we follow the steps of the following Algorithm 1:

Algorithm 1:

1. Consider an initial control $u_k \in \mathcal{U}$ for $k = 0$.
2. Approximate state and adjoint variables, respectively, by solving discrete Equations (40) and (41) with control u_k.
3. Find control u^* using Equation (38).
4. Update the control using $u_k = \dfrac{u^* + u_k}{2}$.
5. If $\delta\|\Theta_k\| - \|\Theta_k - \Theta_{k-1}\| \geq 0$, then stop, otherwise move to step 2.

Here, Θ represents each of the state, adjoint, and control variables, and δ is the required tolerance.

6.1.2. Optimal Quarantine Rates

In this part, we show the simulation results that were attained by resolving the necessary optimality conditions obtained from the fractional-order control problem (36). Steps of Algorithm 1 were carried out using the MATLAB simulation tool, which employs a three-step fractional Adams–Bashforth numerical technique along with RK-4. Table 1 provides the parameter values utilized in simulations. The simulation results are shown for three distinct values of the fractional order ρ, i.e., for $\rho = 0.7,\ 0.8,\ 0.95$.

The main goal of this study was to identify the optimal controls for decreasing COVID-19 in the human population. Figure 13a–c show these optimal behaviors of the curves, respectively, for the time-dependent control variables c_1, c_2, and c_3 for different fractional-orders. Under each set of optimal controls (quarantine rates), the cost function (35) reduced

to its minimum value, as shown in Figure 13d. This result is evident in the solution of the optimal control problem (36). The optimal quarantine rates c_1, c_2, and c_3 have also caused the state variables S, E, I, A, P, Q, H, R to shift from the endemic equilibrium (EE) to the disease-free equilibrium (DFE), as shown in Figure 14.

Thus, our proposed fractional model and the corresponding optimal control strategy of introducing a quarantine compartment suggest that the COVID-19 pandemic can be removed from the society or human population if the infected, asymptomatic, and super-spreaders are quarantined with the rates shown in Figure 13a–c.

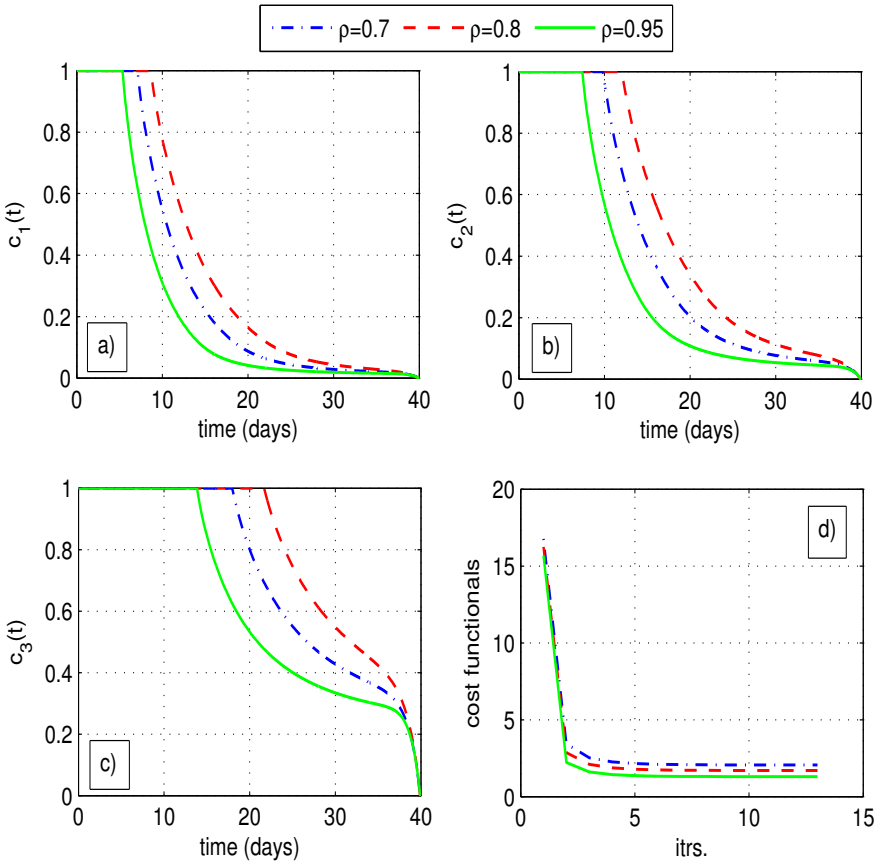

Figure 13. Optimal control variables (quarantine rates) along with the corresponding cost functional for each fractional-order $\rho = 0.7,\ 0.8,\ 0.95$.

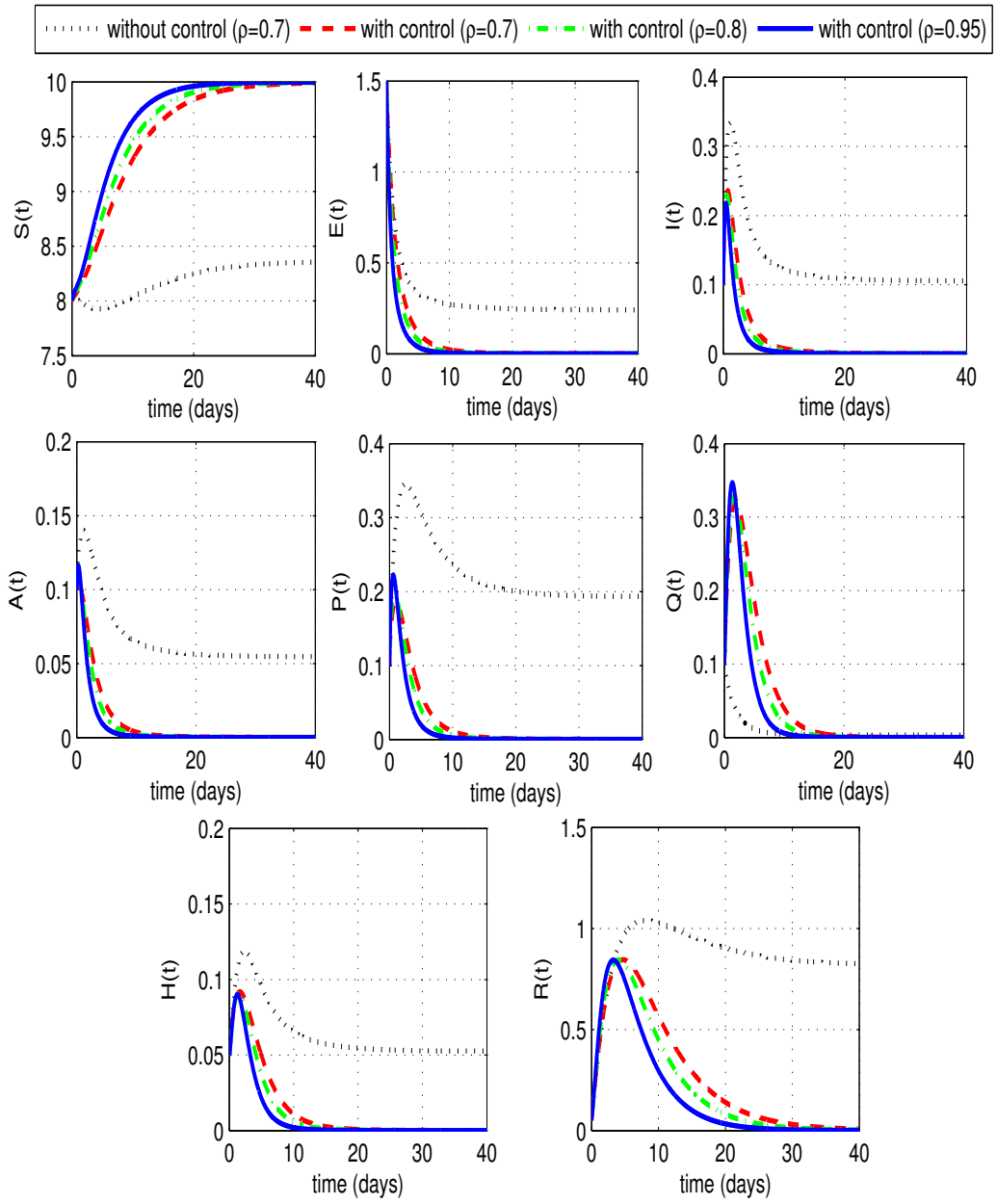

Figure 14. State variables with and without optimal controls.

7. Conclusions

In this study, we designed a nonlinear mathematical model of the COVID-19 pandemic to understand the dynamics of the disease as well as perform the optimal control analysis. For a detailed analysis, we constructed a fractional-order SEIAPHR model in which the infectious compartment was divided into three compartments named symptomatic infectious $I(t)$, asymptomatic infectious $A(t)$, and superspreader $P(t)$. To formulate the proposed model, we used the Caputo–Fabrizio derivative operator that preserves the system's historical memory. The Caputo–Fabrizio derivative operator was used because of its non-singular kernel. Before studying the dynamics of the purposed model, we first proved that the purposed Caputo–Fabrizio fractional model has a unique solution. To prove the existence and uniqueness of the solution, we used well-known results from functional analysis and calculus. After that, we proved the essential biological properties, such as the boundedness and positivity of the solution. For the aspects regarding the future spread of the COVID-19 disease, the reproduction number $\mathcal{R}_0$ is also determined. It is interesting to note that the

reproduction number is the same for the integer-order and fractional-order models. To complete the well-posed property of the suggested model, the stability analyses (local, global) of both equilibrium points are also done with the help of Lyapunov–Castillo's theory. To give the best control strategy, we added a quarantine (isolation) compartment and then proposed a control strategy in two different styles. In the first strategy, we examined the effects of the quarantine rates of $I(t)$, $A(t)$, and $P(t)$ one by one. From the computational results and graphs, we conclude that the quarantine rates c_1 and c_3, respectively, for classes $I(t)$ and $P(t)$ have significant influence in reducing the spread of the disease. If we want to control the disease, we have to focus on these physically meaningful compartments. In the second strategy, we constructed an optimal control problem with a target to determine the best cost-effective quarantine rates that minimize the objective functions in such a way that infections in humans move to disease-free states. The graphical results show that we were successful in determining such time-dependent optimal quarantine rates that can be used to move toward disease-free states.

Author Contributions: Conceptualization, A.I.K.B. and M.A.N.; methodology, A.I.K.B., M.I.; software, A.I.K.B., M.I.; validation, M.I. and S.B.; formal analysis, A.I.K.B., M.I.; investigation, M.A.N., A.I.K.B.; resources, M.A.N., S.B.; data curation, S.B.; writing—original draft preparation, M.I.; writing—review and editing, A.I.K.B., S.B.; visualization, M.I., S.B.; supervision, A.I.K.B., M.A.N.; project administration, A.I.K.B., M.A.N.; funding acquisition, A.I.K.B. All authors have read and agreed to the published version of the manuscript.

Funding: This work was supported by the Deanship of Scientific Research, Vice Presidency for Graduate Studies and Scientific Research, King Faisal University, Saudi Arabia [Project No. GRANT2486].

Data Availability Statement: The data is given in the article with references.

Acknowledgments: The authors would like to acknowledge the support from King Faisal University, Saudi Arabia, project no. GRANT2486.

Conflicts of Interest: The authors declare that they have no competing interests.

References

1. World of Health Organization. Novel Coronavirus (2019-nCoV)-SITUATION REPORT. Available online: https://apps.who.int/iris/bitstream/handle/10665/330760/nCoVsitrep21Jan2020-eng.pdf?sequence=3&isAllowed=y (accessed on 1 January 2023).
2. Bikdeli, B.; Madhavan, M.V.; Jimenez, D.; Chuich, T.; Dreyfus, I.; Driggin, E.; Nigoghossian, C.D.; Ageno, W.; Madjid, M.; Guo, Y.; et al. COVID-19 and thrombotic or thromboembolic disease: Implications for prevention, antithrombotic therapy, and follow-up. *J. Am. Cardiol.* **2020**, *75*, 2950–2973. [CrossRef] [PubMed]
3. Liu, P.-Y.; He, S.; Rong, L.-B.; Tang, S.-Y. The effect of control measures on COVID-19 transmission in Italy: Comparison with Guangdong province in China. *Infect. Dis. Poverty* **2020**, *130*, 9. [CrossRef] [PubMed]
4. Mekonen, K.G.; Balcha, S.F.; Obsu, L.L.; Hassen, A. Mathematical Modeling and Analysis of TB and COVID- 19 Coinfection. *J. Appl. Math.* **2022**, *2022*, 2449710. [CrossRef]
5. Liang, T. Handbook of COVID-19 prevention and treatment, The First Affiliated Hospital, Zhejiang University School of Medicine. *Compil. Accord. Clin. Exp.* **2020**, *68*.
6. Ahmad, W.; Abbas, M.; Rafiq, M.; Baleanu, D. Mathematical analysis for the effect of voluntary vaccination on the propagation of Corona virus pandemic. *Results Phys.* **2021**, *31*, 104917. [CrossRef]
7. Hui, D.S.; Azhar, E.I.; Madani, T.A.; Ntoumi, F.; Kock, R.; Dar, O.; Petersen, E. The continuing 2019-nCoV epidemic threat of novel corona viruses to global health: The latest 2019 novel coronavirus outbreak in Wuhan, China. *Int. J. Infect. Dis.* **2020**, *91*, 264–266. [CrossRef]
8. Volpert, V.; Banerjee, M.; Petrovskii, S. On a quarantine model of Coronavirus infection and data analysis. *Math. Model. Nat. Phenom.* **2020**, *15*, 24. [CrossRef]
9. Mohsen, A.A.; L-Husseiny, H.F.A.; Zhou, X.; Hattaf, K. Global stability of COVID-19 model involving the quarantine strategy and media coverage effects. *AIMS Public Health* **2020**, *7*, 587–605. [CrossRef]
10. De la Sen, M.; Ibeas, A.; Agarwal, R.P. On confinement and quarantine concerns on an SEIAR epidemic model with simulated parameterizations for the COVID-19 pandemic. *Symmetry* **2020**, *12*, 1646. [CrossRef]
11. Chowdhury, A.; Kabir, K.M.A.; Tanimoto, J. How quarantine and social distancing policy can suppress the outbreak of novel coronavirus in developing or under poverty level countries: A mathematical and statistical analysis. *Res. Sq.* **2020**. [CrossRef]
12. Hui, D.S.; Azhar, E.I.; Kim, Y.-J.; Memish, Z.A.; Oh, M.-D.; Zulma, A. Middle East respiratory syndrome coronavirus: Risk factors and determinants of primary, household, and nosocomial transmission. *Lancet Infect. Dis.* **2018**, *18*, 217–227. [CrossRef]

13. Wilder-Smith, A.; Freedman, D.O. Isolation, quarantine, social distancing and community containment: Pivotal role for old-style public health measures in the novel coronavirus (2019-ncov) outbreak. *J. Travel Med.* **2020**, *27*, 1–4. [CrossRef]
14. Rafiq, M.; Macias-Diaz, J.E.; Raza, A.; Ahmed, N. Design of a nonlinear model for the propagation of COVID-19 and its efficient nonstandard computational implementation. *Appl. Math. Model.* **2021**, *89*, 1835–1846. [CrossRef]
15. Gao, Q.; Zhuang, J.; Wu, T.; Shen, H. Transmission dynamics and quarantine control of COVID-19 in cluster community: A new transmission-quarantine model with case study for diamond princess. *Math. Model. Methods Appl. Sci.* **2021**, *31*, 619–648. [CrossRef]
16. Marshall, P. The impact of quarantine on COVID-19 infections. *Epidemiol. Methods* **2021**, *10*, 20200038. [CrossRef]
17. Feng, L.-X.; Jing, S.L.; Hu, S.-K.; Wang, D.-F.; Huo, H.-F. Modelling the effects of media coverage and quarantine on the COVID-19 infections in the UK. *Math. Biosci. Eng.* **2020**, *17*, 3618–3636. [CrossRef]
18. Aronna, M.S.; Guglielmi, R.; Moschen, L.M. A model for COVID-19 with isolation, quarantine and testing as control measures. *Epidemics* **2021**, *34*, 100437. [CrossRef]
19. Acuna-Zegarra, M.A.; Diaz-Infanteb, S.; Baca-Carrasco, D.; Liceaga, D.O. COVID-19 optimal vaccination policies: A modeling study on efficacy, natural and vaccine-induced immunity responses. *medRxiv* **2020**. [CrossRef]
20. Belete, T.M. A review on Promising vaccine development progress for COVID-19 disease. *Vacunas* **2020**, *21*, 121–128. [CrossRef]
21. Kaur, S.P.; Gupta, V. COVID-19 Vaccine: A comprehensive status report. *Virus Res.* **2020**, *288*, 198114. [CrossRef]
22. Shah, A.; Marks, P.W. Unwavering Regulatory Safeguards for COVID-19 Vaccines. *J. Am. Med. Assoc.* **2020**, *324*, 931–932. [CrossRef] [PubMed]
23. Ivanova, P. Russia Says Its Sputnik v Covid-19 Vaccine is 92% Effective. Press Release 11 November 2020. Available online: https://www.reuters.com/article/us-health-coronavirus-russia-vaccine-idCAKBN27R0Z6 (accessed on 1 January 2023).
24. Cohen, E. Moderna's Coronavirus Vaccine is 94.5% Effective, According to Company Data. Press Release Updated 16 November 2020. Available online: https://edition.cnn.com/2020/11/16/health/moderna-vaccine-results-coronavirus/index.html (accessed on 1 January 2023).
25. Yang, W. Modeling COVID-19 pandemic with hierarchical quarantine and time delay. *Dyn. Games Appl.* **2021**, *11*, 892–914. [CrossRef] [PubMed]
26. Ajbar, A.; Alqahtani, R.T.; Boumaza, M. Dynamics of a COVID-19 model with a nonlinear incidence rate, quarantine, media effects, and number of hospital beds. *Symmetry* **2021**, *13*, 947. [CrossRef]
27. Podlubny, I. Fractional differential equations: An introduction to fractional derivatives. In *Fractional Differential Equations, to Methods of Their Solution and Some of Their Applications*; Elsevier: Amsterdam, The Netherlands, 1999.
28. Samko, S.G.; Kilbas, A.A.; Marichev, O.I. *Fractional Integrals and Derivatives: Theory and Applications*; Gordon and Breach Science Publishers: Philadelphia, PA, USA, 1993.
29. Khan, M.F.; Alrabaiah, H.; Ullah, S.; Khan, M.A.; Farooq, M.; Mamat, M.B.; Asjad, M.I. A new fractional model for vector-host disease with saturated treatment function via singular and non-singular operators. *Alex. Eng. J.* **2021**, *60*, 629–645. [CrossRef]
30. Peter, O.J.; Oguntolu, F.A.; Ojo, M.; Oyeniyi, A.O.; Jan, R.; Khan, I. Fractional order mathematical model of monkeypox transmission dynamics. *Phys. Scr.* **2022**, *97*, 084005. [CrossRef]
31. Hadi, M.S.; Bilgehan, B. Fractional COVID-19 Modeling and Analysis on Successive Optimal Control Policies. *Fractal Fract.* **2022**, *6*, 533. fractalfract6100533. [CrossRef]
32. Shaikh, A.S.; Shaikh, I.N.; Nisar, K.S. A mathematical model of COVID-19 using fractional derivative: Outbreak in India with dynamics of transmission and control. *Adv. Differ. Equations* **2020**, *2020*, 373. [CrossRef]
33. Ali, Z.; Rabiei, F.; Rashidi, M.M.; Khodadadi, T. A fractional-order mathematical model for COVID-19 outbreak with the effect of symptomatic and asymptomatic transmissions. *Eur. Phys. J. Plus* **2022**, *137*, 395 . [CrossRef]
34. Tunç, O.; Tunç, C. Solution estimates to Caputo proportional fractional derivative delay integro-differential equations. *Rev. R. Acad. Cienc. Exactas Fís. Nat. Ser. A Mat. RACSAM* **2023**, *117*, 12. [CrossRef]
35. Tunç, C.; Tunç, O.; Yao, J.-C. On the new qualitative results in integro-differential equations with Caputo fractional derivative and multiple kernels and delays. *J. Nonlinear Convex Anal.* **2022**, *23*, 2577–2591. [CrossRef]
36. Butt, A.I.K.; Chamaleen, M.I.D.B.D.; B, S. Optimal control strategies for the reliable and competitive mathematical analysis of COVID-19 pandemic model. *Math. Meth. Appl. Sci.* **2023**, *46*, 1528–1555.
37. Losada, J.; Nieto, J.J. Properties of a new fractional derivative without singular kernel. *Prog. Fract. Differ. Appl.* **2015**, *1*, 87–92. [CrossRef]
38. Caputo, M.; Fabrizio, M. A new definition of fractional derivative without singular kernel. *Prog. Fract. Differ. Appl.* **2015**, *1*, 73–85.
39. Hanif, A.; Butt, A.I.K.; Ahmad, S.; Din, R.U.; Mustafa Inc. A new fuzzy fractional-order model of transmission of COVID-19 with quarantine class. *Eur. Phys. J. Plus* **2021**, *136*, 1179.
40. Ahmad, W.; Abbas, M. Effect of quarantine on transmission dynamics of Ebola virus epidemic: A mathematical analysis. *Eur. J. Plus* **2021**, *136*, 355. [CrossRef]
41. Ahmad, W.; Rafiq, M.; Abbas, M. Mathematical analysis to control the spread of Ebola virus epidemic through voluntary vaccination. *Eur. Phys. J. Plus* **2020**, *135*, 775. [CrossRef]
42. Rafiq, M.; Ahmad, W.; Abbas, M.; Baleanu, D. A reliable and competitive mathematical analysis of Ebola epidemic model. *Adv. Differ. Equations* **2020**, *2020*, 540. [CrossRef]

43. Butt, A.I.K.; Abbas, M.; Ahmad, W. A mathematical analysis of an isothermal tube drawing process. *Alexanderia Eng. J.* **2020**, *59*, 3419–3429. [CrossRef]
44. Castillo-Chavez, C.; Feng, Z.; Huanz, W.; Driessche, P.V.D.; Kirschner, D.E. On the computation of RO and its role in global stability. In *Mathematical Approaches for Emerging and Reemerging Infectious Diseases: An Introduction*; Springer: Berlin/Heidelberg, Germany, 2002. [CrossRef]
45. Thabet, S.T.M.; Abdo, M.S.; Shah, K. Theoretical and numerical analysis for transmission dynamics of COVID-19 mathematical model involving Caputo-Fabrizio derivative. *Adv. Differ. Equ.* **2021**, *2021*, 184
46. Vargas-De-Len, C. Volterra-type Lyapunov functions for fractional-order epidemic systems. *Commun. Nonlinear Sci. Numer. Simul.* **2015**, *24*, 75–85. [CrossRef]
47. Moore, E.J.; Sirisubtawee, S.; Koonprasert, S. A Caputo-Fabrizio fractional differential equation model for HIV/AIDS with treatment compartment. *Adv. Differ. Equations* **2019**, *2019*, 200. [CrossRef]
48. Lenhart, S.; Workman, J.T. *Optimal Control Applied to Biological Models*; Chapman & Hall/CRC: Boca Raton, FL, USA, 2007. [CrossRef]
49. Wang, H.; Jahanshahi, H.; Wang, M.K.; Bekiros, S.; Liu, J.; Aly, A.A. A Caputo-Fabrizio fractional-order model of HIV/AIDS with a treatment compartment: Sensitivity analysis and optimal control strategies. *Entropy*, **2021**, *23*, 610.